Adult Acquired Flatfoot Deformity: Anatomy, Biomechanics, Staging, and Imaging Findings

Dyan V. Flores, MD
Catalina Mejía Gómez, MD
Moisés Fernández Hernando, MD
Michael A. Davis, MD
Mini N. Pathria, MD

Abbreviations: AAFD = adult acquired flatfoot deformity, PTT = posterior tibialis tendon

RadioGraphics 2019; 39:1437–1460

https://doi.org/10.1148/rg.2019190046

Content Codes: MK MR

From the Department of Radiology, Philippine Orthopedic Center, St. Luke's Medical Center–Global City, Maria Clara St, Santa Mesa Heights, Quezon City, Metro Manila, Philippines 1100 (D.V.F.); Department of Radiology, Hospital Pablo Tobón Uribe, Medellín, Colombia (C.M.G.); Department of Radiology, Diagnóstico Médico Cantabria, Santander, Spain (M.F.H.); Department of Radiology, University of Texas Health Science Center, San Antonio, Texas (M.A.D.); and Department of Radiology, UCSD Health System, San Diego, Calif (M.N.P.). Recipient of a Magna Cum Laude award for an education exhibit at the 2018 RSNA Annual Meeting. Received March 7, 2019; revision requested April 26 and received May 13; accepted May 24. For this journal-based SA-CME activity, the authors, editor, and reviewers have disclosed no relevant relationships. **Address correspondence to** D.V.F. (e-mail: *dyanflores@yahoo.com*).

SA-CME LEARNING OBJECTIVES

After completing this journal-based SA-CME activity, participants will be able to:

- Describe the anatomy and function of each of the principal stabilizers of the medial arch and how their dysfunction leads to AAFD.
- Assess foot malalignment with standard radiographic metrics and recognize imaging findings that indicate damage to the supporting structures of the foot.
- Explain the principles of clinical staging of AAFD and the most commonly used treatment options for each stage.

See rsna.org/learning-center-rg.

Adult acquired flatfoot deformity (AAFD) is a common disorder that typically affects middle-aged and elderly women, resulting in foot pain, malalignment, and loss of function. The disorder is initiated most commonly by degeneration of the posterior tibialis tendon (PTT), which normally functions to maintain the talonavicular joint at the apex of the three arches of the foot. PTT degeneration encompasses tenosynovitis, tendinosis, tendon elongation, and tendon tearing. The malaligned foot is initially flexible but becomes rigid and constant as the disorder progresses. Tendon dysfunction commonly leads to secondary damage of the spring ligament and talocalcaneal ligaments and may be associated with injury to the deltoid ligament, plantar fascia, and other soft-tissue structures. Failure of multiple stabilizers appears to be necessary for development of the characteristic planovalgus deformity of AAFD, with a depressed plantar-flexed talus bone, hindfoot and/or midfoot valgus, and an everted flattened forefoot. AAFD also leads to gait dysfunction as the foot is unable to change shape and function adequately to accommodate the various phases of gait, which require multiple rapid transitions in foot position and tone for effective ambulation. The four-tier staging system for AAFD emphasizes physical examination findings and metrics of foot malalignment. Mild disease is managed conservatively, but surgical procedures directed at the soft tissues and/or bones become necessary and progressively more invasive as the disease progresses. Although much has been written about the imaging findings of AAFD, this article emphasizes the anatomy and function of the foot's stabilizing structures to help the radiologist better understand this disabling disorder.

Online supplemental material is available for this article.

Introduction

Flatfoot is a common concern of patients who present in any musculoskeletal practice. The condition, which is often referred to as pes planus, planovalgus foot, or simply as fallen arches, can be developmental or acquired (1). Developmental flatfoot is normal in toddlers and occasionally persists into adulthood without symptoms. Although childhood flatfoot typically is related to immaturity, it can be associated with coalition, neuromuscular disease, laxity syndromes, and numerous other causes (2). Acquired flatfoot is characterized by partial or complete flattening of the medial arch that develops after skeletal maturity (3). It may be relatively asymptomatic, or it may lead to profound symptoms and dysfunction that are disabling enough to incapacitate patients. There are myriad causes of acquired flatfoot, including posterior tibialis tendon (PTT) degeneration, trauma, neuroarthropathy, neuromuscular disease, and inflammatory arthritis. Of these, PTT degeneration is, by far, the most common. Initially,

TEACHING POINTS

- The cumulative damage of multiple structures causes the typical malalignment of AAFD, with a flattened medial arch, peritalar subluxation, and an externally rotated foot that is elongated medially and shortened laterally.
- Tendon degeneration occurs along a continuum from synovial and peritendinous inflammation, to tendinosis, to partial tearing, to complete tearing; these stages often overlap within the same tendon.
- The spring ligament, also known as the plantar calcaneonavicular ligament, is considered the primary static stabilizer of the medial arch and is second in importance only to the PTT.
- Staging is primarily based on objective findings (the presence or absence of deformity, whether deformity is flexible or rigid, the presence or absence of secondary osteoarthrosis) rather than symptoms.
- AAFD most commonly is caused by a cascade of abnormalities in the foot that start with PTT dysfunction and ultimately lead to damage of other supporting soft tissue, malalignment, gait abnormality, and arthrosis.

this condition was referred to as posterior tibialis tendon dysfunction, but more recently it has been termed adult acquired flatfoot deformity (AAFD), because its abnormality is not limited to the PTT but encompasses a host of soft-tissue abnormalities at the posteromedial and plantar foot (4,5) (Fig 1). Imaging is important in the assessment of AAFD to exclude underlying conditions leading to flatfoot, evaluate the soft-tissue structures responsible for the disorder, recognize complications related to their dysfunction, and stage the disease and guide selection of the optimal therapy.

Figure 1. Clinical appearance of AAFD in a 49-year-old man. Photograph of the medial foot shows lowering of the medial longitudinal arch while the patient is standing, with the entire sole in contact with the ground. Although there is no strict clinical definition of flatfoot, the medial arch is normally tall enough to accommodate an examiner's fingertips easily. Note the prominence of the talar head (*), which has descended because of failure of the supporting structures of the medial foot and valgus deviation of the midfoot and forefoot. Reappearance of the arch while the patient is sitting and standing on the toes indicates a flexible deformity, whereas persistence of arch collapse in all postures is referred to as rigid flatfoot.

Normal Foot

The foot has 26 bones, 10 major extrinsic tendons, more than 30 joints, and numerous intrinsic myotendinous units and ligaments arranged together to form three arches (1,6). These structures must work in concert throughout life to allow the foot to support standing weight and absorb impact, store and release energy, and adapt to shifting loads during activity (7).

Arches of the Foot

The foot is constructed as a series of three intersecting arches: a longitudinal lateral arch, a longitudinal medial arch, and a transverse arch at the level of the distal tarsal bones (Fig 2). These arches are interrelated, so failure at one leads to dysfunction at the others (8,9). The lateral arch, which is composed of the calcaneus, cuboid bone, and fourth and fifth metatarsals, is rigid and functions to support body weight (8). The medial arch, comprising the calcaneus, talus, navicular, and cuneiform bones and the medial three metatarsals, is taller and more flexible, which allows it to vary dynamically in shape and

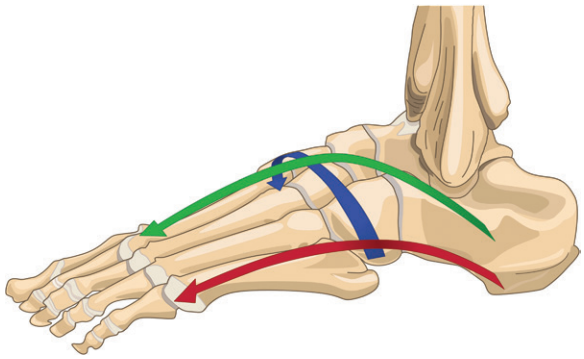

Figure 2. Illustration of the three intersecting arches of the foot. The longitudinal lateral arch (red) is relatively flat compared with the longitudinal medial arch (green). The transverse arch (blue) at the tarsometatarsal region runs perpendicular to the longitudinal arches and is taller medially than it is laterally. The talonavicular joint normally is located at the vault of the curved plane formed by these arches, and therefore it is the highest point of the foot.

configuration during gait (1,6,8). The osseous structures that form the longitudinal arches are referred to as the lateral and medial columns of the foot. The transverse arch is most commonly described as comprising the metatarsal bases and cuneiform and cuboid bones. Some authors recognize an additional transverse arch at the metatarsal heads, while Gray (10) described a series of transverse arches at the foot, recognizing that the three arches act akin to the edges of a sail, forming a curved domelike structure with its apex at the medial midfoot. The apex of the intersection of the three arches is the transverse tarsal or midtarsal joint (talonavicular and calcaneocuboid articulations) with the talonavicular

Table 1: Commonly Used Radiographic Metrics of Foot Alignment

Metric	Construction	Alignment Angle (degrees)	
		Normal	Abnormal
Lateral view: assessment of longitudinal arch			
Talus–first metatarsal angle (Meary angle)	Angle between the long axis of the talus and the long axis of the first metatarsal	0 (parallel)	Mild: >4 Moderate: >15 Severe: >30
Calcaneal inclination angle	Angle between the line at the plantar calcaneal surface and the horizontal plane	20–30	Pes planus: <18
Calcaneal–fifth metatarsal angle	Angle between the line at the plantar calcaneal surface and the line at the inferior fifth metatarsal shaft	150–165	>170
Anteroposterior view: assessment of heel valgus and forefoot abduction			
Talocalcaneal angle (kite angle)	Angle between the line bisecting the head and neck of the talus and the line parallel to the lateral surface of the calcaneus	>25–40	>40 (heel valgus) <25 (heel varus)
Talus–first metatarsal alignment	Line drawn along the long axis of the talus, extended into the forefoot, its orientation compared with that of the first metatarsal shaft	Talar axis angled slightly lateral to the shaft	Talar axis angled medial to the shaft
Talonavicular coverage angle	Angle between the articular surface of the talar head and the articular surface of the proximal navicular bone	0 (parallel)	>7

joint acting as the keystone of the triple arch complex (4,11).

Infants are born with abundant plantar fat and flexible flat feet without any arch, which often engenders unnecessary parental distress (12–14). The arches develop rapidly when the child is 3–6 years old, with the medial arch appearing first, and the other arches maturing until growth ceases (12,14). Factors necessary for successful arch development include appropriate ossification, particularly at the sustentaculum tali and navicular bone; healthy soft-tissue stabilizers; proper plantar fascial tone; and a noncontracted Achilles tendon (15). Up to 15% of the population never develop well-defined arches. Developmental flatfoot among adults is considered physiologic unless the person becomes symptomatic (16,17). An estimated 7%–15% of adults with developmental flatfoot eventually develop symptoms that lead them to seek medical attention (16).

Normal Alignment

Radiography is used commonly for measuring foot alignment. In the context of AAFD, measurements are used principally to evaluate longitudinal arch flattening, hindfoot valgus, and forefoot abduction (Table 1). The most commonly used metrics for the longitudinal arch are the Meary angle, the calcaneal inclination angle, and the calcaneal–fifth metatarsal angle (Fig 3). The most common metrics for hindfoot valgus and forefoot abduction are the talocalcaneal angle (kite angle), the talus bone–first metatarsal axis, and the talonavicular angle (Fig 4). While these techniques suffice for most patients, numerous other parameters of alignment are described (18–20). The preferred method of assessment of alignment is radiography of the weight-bearing foot, because flexible deformity may not be apparent without loading. While anteroposterior and lateral views are usually sufficient, specialized projections such as the hindfoot alignment or a long axial view are used in selected patients (21,22). Weight-bearing footprint analysis and pressure maps are appealing visual aids but are not used routinely. Although CT and MRI are used to describe alignment, these techniques are not performed with the patient in a weight-bearing position and are insensitive until the deformity becomes inflexible (23) (Fig 5).

Stabilizers

The geometry of the osseous structures contributes to arch alignment and stability, but the bone configuration alone is insufficient. Soft-tissue stabilizers are required; these act in concert and reinforce each other during standing and gait. The posterior tibialis muscle is the principal dynamic

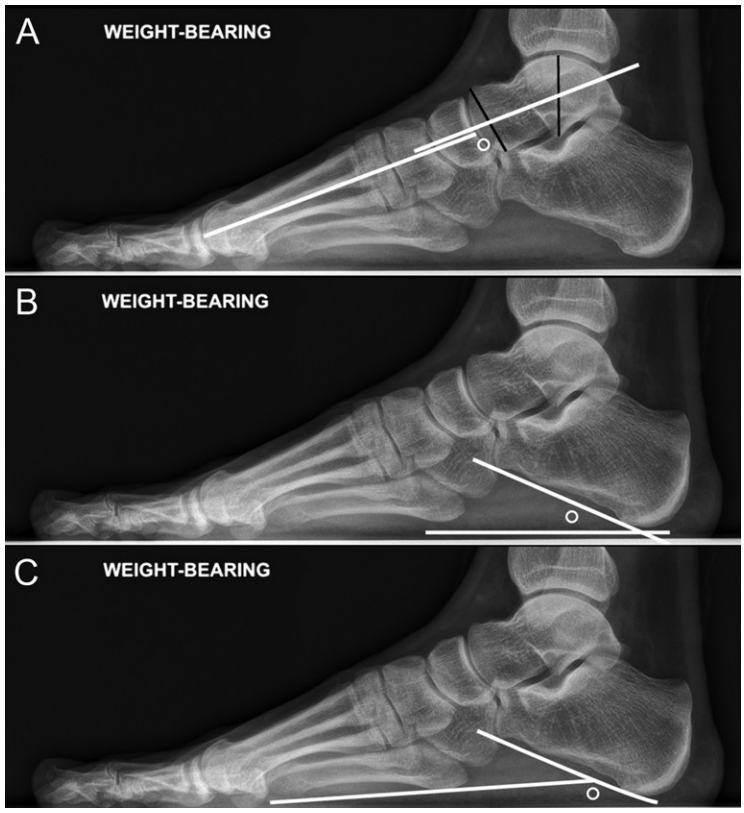

Figure 3. The three most commonly used measurements of foot alignment and arch integrity in a normal foot. *A,* Lateral radiograph shows the Meary angle between the axis of the talus bone and that of the first metatarsal. These axes are normally parallel and typically overlap, forming a nearly continuous line. The Meary angle is sensitive for diagnosis of AAFD, because it measures structures located at the medial column. *B,* Lateral radiograph shows the calcaneal inclination angle (or the calcaneal pitch angle), which is the angle between the inferior calcaneus and the horizontal plane. *C,* Lateral radiograph shows the calcaneus–fifth metatarsal angle, which is the angle between the inferior calcaneus and the inferior surface of the fifth metatarsal. Both structures are located at the lateral column.

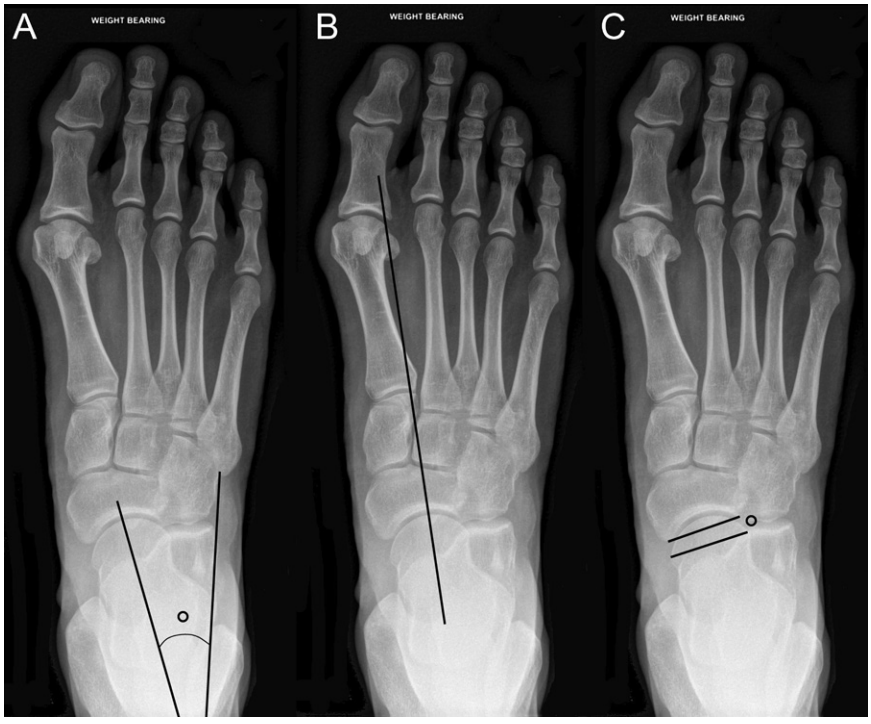

Figure 4. Three commonly used measurements of foot alignment in a normal foot. *A,* Anteroposterior radiograph shows the kite angle, which is formed by the intersection of a line drawn at the midtalus and a line along the lateral margin of the calcaneus and is used to assess heel valgus. Heel valgus also can be assessed by measuring the talocalcaneal angle on lateral images. *B,* Anteroposterior radiograph shows the talometatarsal relationship, which is assessed by drawing lines along the long axes of the first metatarsal and the talar axis. These are normally in line; medial angulation of the talar axis with respect to that of the metatarsal shaft is abnormal. This measurement should not be used if substantial hallux valgus is present. *C,* Anteroposterior radiograph shows the talonavicular coverage angle, which is the angle between the margins of the articular surfaces of the talar head and the navicular bone. It is a useful metric for evaluating lateral rotation of the navicular bone relative to the talus bone.

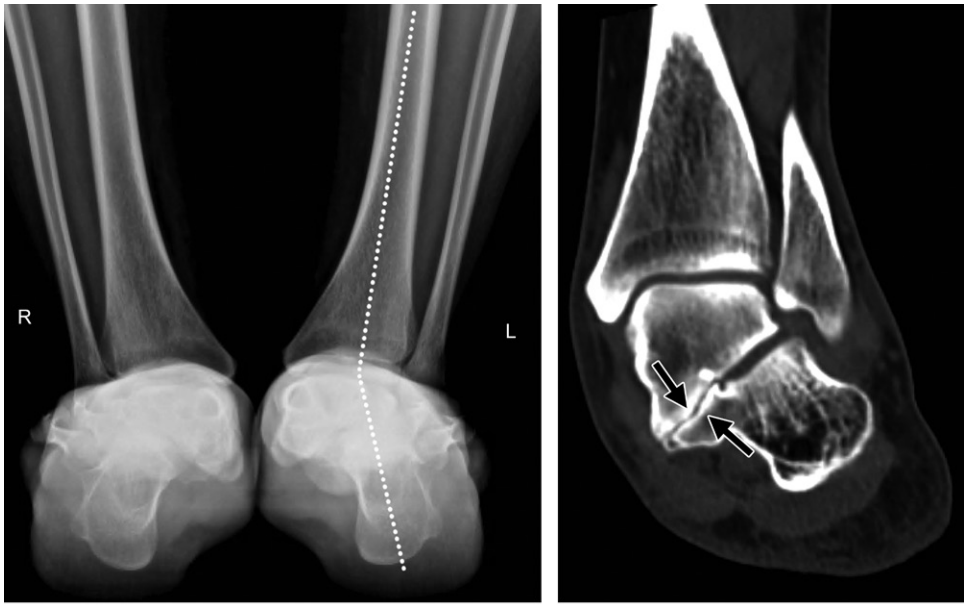

a. b.

Figure 5. Heel valgus in a 43-year-old woman who described being flatfooted since childhood but recently became more symptomatic. **(a)** Standing hindfoot alignment radiograph shows an abnormal tibiocalcaneal angle (greater than 5°) bilaterally (illustrated on the left ankle by the dotted line). This view allows assessment of the calcaneal valgus relative to the tibia in the coronal plane. **(b)** Corresponding CT image of the left hindfoot shows a fibrocartilaginous coalition at the middle facet of the subtalar joint (arrows) with narrowing and downsloping of the articulation and heel valgus, indicating that the deformity is inflexible. A similar coalition was present on the right (not shown).

stabilizer, with lesser contributions from the flexor digitorum longus, flexor hallucis longus, peroneus longus, and gastrocnemius and soleus muscles by means of their fascial connections with the calcaneus and plantar fascia (1,6,7). The intrinsic foot muscles also contribute by sensing deformation and providing rapid local stabilization (7). The most important static stabilizers are the spring ligament, talocalcaneal ligaments, deltoid ligaments, plantar fascia, and tarsometatarsal joint complex (6,8) (Table 2).

The abnormal anatomy of AAFD typically starts at the PTT, but dysfunction in this tendon by itself is not enough to lead to substantial deformity (17,24–27). Instead, PTT failure leads to overload and predictable abnormalities in the remaining supporting structures, most importantly at the spring ligament and the talocalcaneal ligaments at the sinus tarsi. The cumulative damage of multiple structures causes the typical malalignment of AAFD, with a flattened medial arch, peritalar subluxation, and an externally rotated foot that is elongated medially and shortened laterally (3,9,16,17).

Posterior Tibialis Tendon

Anatomy

The posterior tibialis is the deepest and most central of the calf muscles, originating from the proximal tibia, fibula, and interosseous membrane. The tendon forms above the ankle and turns from a vertical to a more horizontal orientation at the medial malleolus, where it is held firmly in the retromalleolar groove by the flexor retinaculum, forming a fibro-osseous pulley (16,28–30) (Fig 6). A 1–2-cm avascular segment is described behind the malleolus, where the intratendinous vessels lack anastomoses (31). The tendon trifurcates alongside the medial talus bone proximal to the navicular bone. The main division, which is formed from the anterior two-thirds of the tendon, contains the fibers that form the PTT's principal insertion at the navicular tuberosity and fibers that insert at the medial cuneiform bone (16,32). There is some variability in the insertions of its smaller plantar and recurrent divisions. These typically include the second and third cuneiform bones, the plantar bases of the second to fourth metatarsals, the cuboid bone, the sustentaculum tali, and numerous less-consistent insertions onto regional muscles, tendons, and ligaments (30,32).

Function and Dysfunction

By virtue of the tendon's position posteromedial to the ankle joint and medial to the subtalar axis, the PTT functions as both a plantar flexor and an inverter of the foot (1,16,17). As a plantar flexor, it functions in coordination with the flexor digitorum longus and flexor hallucis longus tendons and

Table 2: Stabilizing Structures of the Foot

Structure	Function	Signs of Failure
Primary structure: posterior tibialis tendon	Plantar flexion of the navicular and midfoot relative to the talus Hindfoot inversion Locking of the medial arch during gait Forefoot adduction (counteracts peroneus brevis)	Talar head plantar flexion Overloaded spring ligament Hindfoot valgus Overloaded talocalcaneal ligaments Navicular descent Everted calcaneus (malalignment of the Achilles tendon) Forefoot abduction Overloaded tarsometatarsal joints
Secondary structures		
Spring ligament	Support for the head of the talus	Talar descent Talar plantar flexion
Talocalcaneal ligaments	Maintenance of talocalcaneal alignment and subtalar stability	Talocalcaneal instability Sinus tarsi syndrome
Deltoid ligaments		
Superficial	Resistance of lateral translation and eversion of the talus	Inward displacement of the talar head Hindfoot valgus and pronation
Deep	Limitation of the tibiotalar valgus	Tibiotalar malalignment and arthrosis
Plantar fascia	Prevention of elongation of the plantar foot (truss) Elevation of the arch by drawing the calcaneus and metatarsal heads together (windlass)	Flattening of the plantar foot at midstance Ineffective arch rise during the late stance period of gait
Tarsometatarsal joints	Maintenance of the transverse arch Maintenance of tarsometatarsal alignment	Flattening of the transverse arch, impacting the medial arch apex Tarsometatarsal subluxation and arthrosis

the gastrocnemius-soleus complex (28). As an inverter, the tendon acts to adduct and supinate the foot simultaneously (16,17). Although the PTT has insertions onto virtually every other structure at the midfoot, it lacks an attachment to the talus bone. The normal PTT effectively draws the rest of the medial and plantar midfoot relative to the talus bone, supporting the talar head and preventing it from descending. Failure of the tendon allows the rest of the foot to migrate away from the talus bone, leading to peritalar subluxation and malalignment (Fig 7).

During quiet standing, the posterior tibialis is relatively quiet, although it contributes to maintaining proper tension of the secondary stabilizers by means of its distal attachments at these structures (16,17). It is during gait that a properly functioning PTT is critical to stabilizing the medial arch and establishing proper alignment for effective activity (10,16). Some basic understanding of the gait cycle helps in understanding the dysfunction associated with AAFD (1,11).

The gait cycle describes the series of events that take place during one stride, in the following example, at the right foot (Fig 8). Each stride consists of a stance phase and a swing phase. During the stance phase, the right foot is weight bearing,

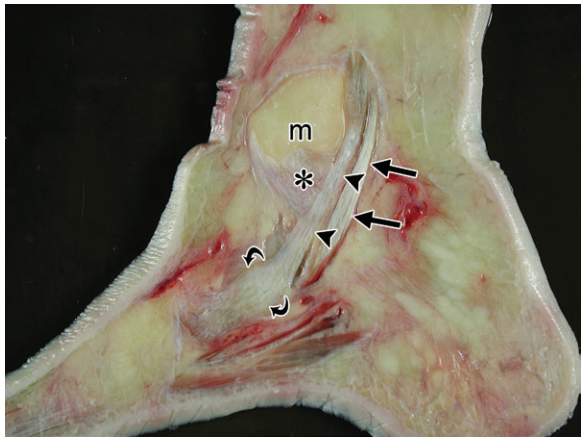

Figure 6. Cadaveric anatomic slice through the medial ankle. Sagittal photograph of a slice through the medial malleolus *(m)* shows the PTT (arrowheads) located immediately posterior to the malleolus, with the flexor digitorum longus tendon (straight arrows) posterior to it. The angular change and relative avascularity of the PTT at the malleolus make the tendon vulnerable to degeneration. Note the broadening of the PTT distally at its navicular attachment (curved arrows). Portions of the deltoid ligament are visible arising from the medial malleolus (*). (Image courtesy of Donald Resnick, MD, University of California, San Diego, Calif.)

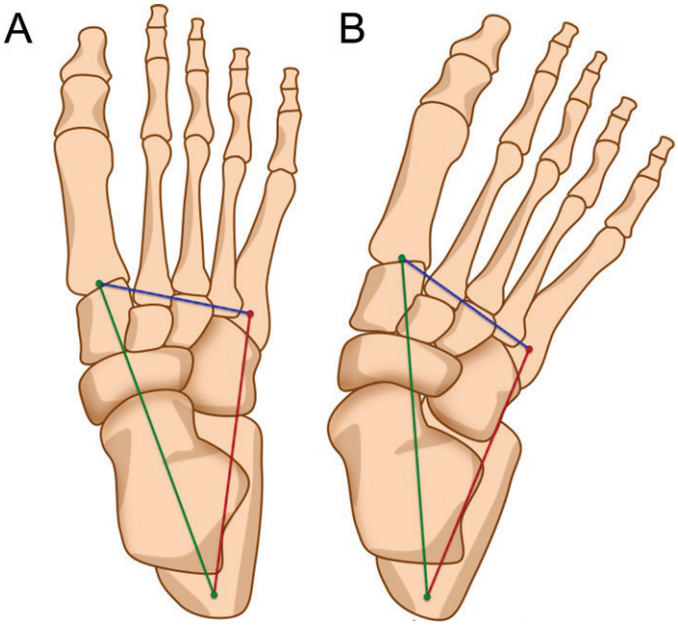

Figure 7. Normal alignment and malalignment in AAFD. Illustration shows, *A,* normal foot alignment and, *B,* malalignment related to AAFD. When the PTT is dysfunctional or torn, it is no longer able to invert and plantar flex the midfoot structures relative to the talus bone, and they rotate externally. The talus bone itself cannot rotate as long as the tibiotalar joint is intact. Instead, the talar head plantar flexes and descends as it becomes uncovered and loses the support of the rest of the foot. In AAFD, note that the talonavicular joint is no longer aligned within the three arches of the foot (colored lines), disrupting normal biomechanics.

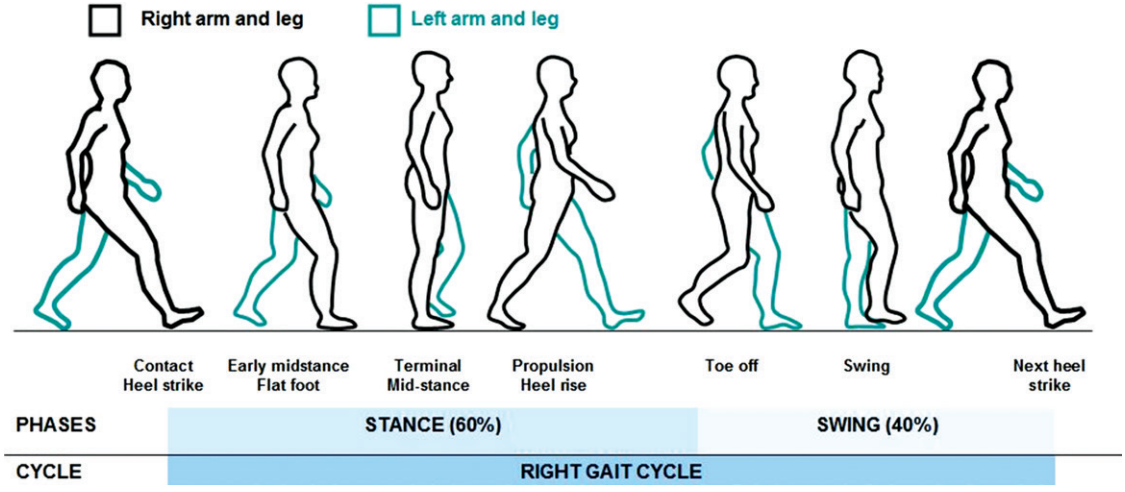

Figure 8. Simplified illustration of the gait cycle, which consists of a stance phase and a swing phase. The PTT is only active during the stance phase, which makes up 60% of the duration of each cycle. The stance phase consists of the heel strike (right heel contacts the ground anterior to the body), flat foot (the entire right foot on the ground), and heel rise (the right heel elevates off the ground posterior to the body). At midstance, the foot is in the flatfoot stage, with the contralateral foot off the ground. During the swing phase, the foot is off the ground and swings anterior to the body in preparation for the next heel strike.

and body weight is shifting forward over it. This phase is composed of three principal stages: contact (heel strike), midstance (flat foot), and propulsion (heel rise). Midstance is further divided into a foot-flat phase and a terminal stance phase, during which the foot prepares for propulsion (11). The stance phase ends with toe-off, when the right foot leaves the ground to enter the swing phase, during which the right foot is unloaded.

The PTT is active only during the stance phase. At heel strike, the hindfoot is in valgus, and the midfoot and forefoot are in supination and abduction. The PTT undergoes eccentric contraction, allowing a smooth transition from supination to pronation and a shift of weight from the heel to the forefoot (4,27). At midstance, while the right foot is flat and the left is elevated, the support structures act synergistically to maintain the arches and support body weight. During terminal midstance, concentric contraction of the PTT inverts the hindfoot; inversion of the subtalar joint causes the foot to become less flexible, thereby "locking" the midtarsal joint (11). This locking occurs just as concentric contraction of the gastrocnemius and soleus muscles starts to plantar flex the ankle and lift the heel. By locking the midtarsal joint, the PTT creates a rigid lever so that plantar flexion generated by the gastrocnemius and soleus muscles at the ankle is translated through the arch to the metatarsal

Figure 9. Bone proliferation at the medial malleolus secondary to a chronic PTT abnormality in a 51-year-old woman. **(a)** Anteroposterior radiograph shows irregular bone proliferation at and above the medial malleolus (arrows) and medial soft-tissue swelling, which is most apparent below the malleolus. **(b)** Corresponding coronal fat-suppressed proton-density-weighted MR image shows bone hypertrophy and marrow edema at the malleolus (arrowheads). The PTT is thickened with intrasubstance tearing, and there is considerable fluid surrounding the tendon, indicating tenosynovitis.

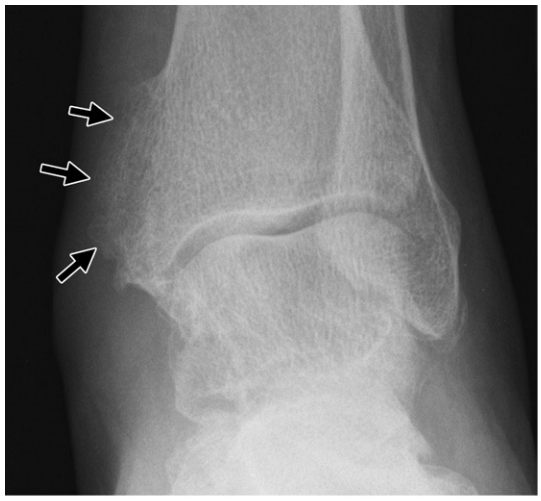

a.

b.

heads (1,17,33). Inversion also medializes the gastrocnemius-soleus axis so that the propulsive force of the Achilles tendon is directed maximally toward the first tarsometatarsal joint in preparation for toe-off (1,34,35). In a patient with PTT deficiency, inactivity of the PTT during heel rise allows the foot to remain everted during contraction of the gastrocnemius-soleus complex, which then becomes a subtalar pronator rather than a supinator. Pronation of the subtalar joint unlocks the midtarsal joint, which is already destabilized by attenuation of the PTT, particularly the critical talonavicular joint (11). The concentric force of the gastrocnemius and soleus muscles is then able to create a plantar flexion moment at the flexible midtarsal joint, resulting in plantar flexion of the hindfoot with respect to the forefoot and overloading of the attenuated PTT. Over time, the unlocked midtarsal joint succumbs to deforming forces of body weight, and the gastrocnemius and soleus muscles and the static supporting structures stretch and fail (11,34).

PTT Abnormalities

PTT abnormalities are most common in middle-aged and elderly women and are caused by repetitive overloading, which leads to progressive tendon degeneration. Preexisting developmental flatfoot, obesity, diabetes, gout, inflammatory arthropathy, and the use of corticosteroids are associated risk factors (28,33,36). Symptoms of pain, swelling, malalignment, and gait dysfunction develop and progress as tendon degeneration advances. Tendon degeneration occurs along a continuum from synovial and peritendinous inflammation, to tendinosis, to partial tearing, to complete tearing; these stages often overlap within the same tendon (5,37). A degenerated tendon may be elongated and dysfunctional without an actual tear (5,38). Although elongation by as little as 1 cm markedly reduces the effectiveness of the tendon, length change and laxity are challenging to recognize with standard imaging techniques, and this leads to discrepancies between clinical status and imaging findings (17,24). In rare cases, the PTT is acutely injured during activities requiring abrupt changes in direction that cause differential movements at the tendon's multiple insertions (39,40). Acute injury can result in midsubstance tendon tearing, insertional avulsion at the navicular bone, or tendon dislocation at the malleolus (30).

Imaging of PTT Degeneration

Although radiography is used primarily to assess alignment, secondary findings indicating tendon disease such as swelling, navicular bone tuberosity enthesopathy, and bone hypertrophy at the retromalleolar groove also should be noted (9,38,41). Peritendinous proliferative changes at the distal tibia can be pronounced, sometimes simulating a sessile osteochondroma at radiography and producing considerable marrow edema at MRI (Fig 9). The PTT is well assessed with US (29,42,43). Hypoechoic fluid surround-

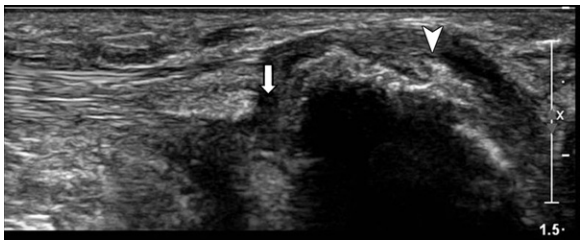

Figure 10. Insertional tear of the PTT in a 67-year-old man. Long-axis US image through the distal PTT shows thickening, irregularity, and signal intensity heterogeneity of the tendon near its navicular bone insertion. There is low-grade interstitial tearing of the tendon at its insertion (arrow) and enthesopathy at the medial navicular bone (arrowhead). The tendon appears more normal proximally over the talus bone.

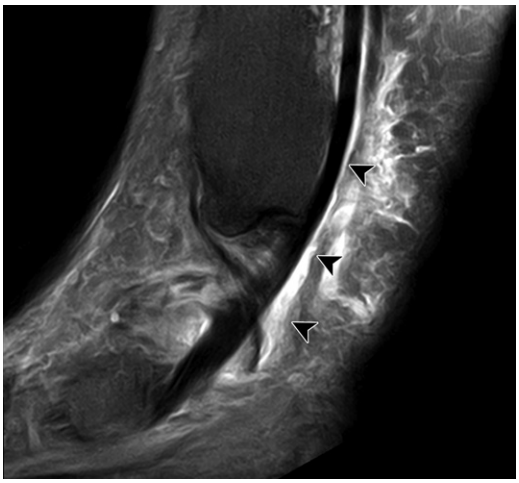

Figure 12. PTT tenosynovitis in a 52-year-old woman with chronic medial retromalleolar pain predominantly at night and during walking. Sagittal fat-suppressed T2-weighted MR image obtained at the medial malleolus shows the PTT outlined by excessive fluid in its tendon sheath (arrowheads) and surrounding soft-tissue inflammation.

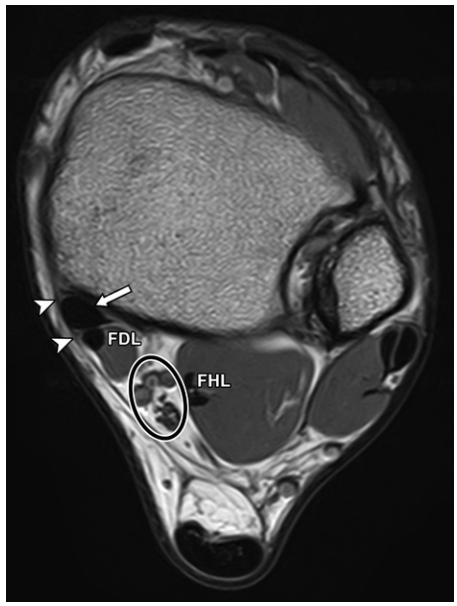

Figure 11. Normal PTT at the level of the medial malleolus in a 42-year-old man. Axial T1-weighted MR image of the normal ankle shows the normal PTT located behind the medial malleolus (arrow), which is covered by the flexor retinaculum (arrowheads). The smaller flexor digitorum longus (*FDL*) and flexor hallucis longus (*FHL*) tendons lie posterolateral to the PTT, with the tibial neurovascular bundle (oval outline) located between them. The PTT is best evaluated in this plane, with the sagittal and coronal planes serving as useful adjuncts for abnormalities remote from the malleolus.

ing the tendon and a sheath size of greater than 7 mm indicate tenosynovitis (16). Tendinosis results in thickening, with heterogeneous hypoechoic regions replacing the normal fibrillar architecture and hypervascularity at color Doppler US. Tears appear as clefts or gaps in a tendinotic tendon and are often associated with caliber alterations (38) (Fig 10). Dynamic US is useful in patients suspected of having friction syndrome at a thickened retinaculum and tendon instability related to flexor retinaculum disruption, which allows anterior tendon subluxation (29,38,42).

MRI is the preferred modality for assessment of the PTT, and it has good accuracy for showing tendon abnormalities while allowing comprehensive evaluation of other soft-tissue and osseous structures (24,29,44). The normal PTT is the largest and most medial of the three flexor tendons and appears as an ovoid low-signal-intensity structure with a transverse diameter of 7–11 mm, which is approximately twice that of the adjacent flexor digitorum longus muscle(30,44,45) (Fig 11). Near its navicular bone insertion, the PTT normally enlarges and may appear heterogeneous because of intratendinous fibrocartilage or connective tissue interposed between its divisions (28,40,46).

Tenosynovitis appears as fluid and/or synovitis surrounding the tendon distending a normal or thickened sheath, often with adjacent edema (Fig 12). The sheath ends 1–2 cm proximal to the navicular bone, so fluid around the distal tendon can be described as paratenonitis (30). Tenosynovitis and paratenonitis, in the absence of tendon abnormality, correlate poorly with quantitative assessments of foot malalignment (41,47).

Tendinosis, the most common abnormality that affects the tendon, causes thickening, surface irregularity, and heterogeneous intratendinous signal intensity that is less intense than that of fluid. The "magic angle" artifact, which occurs where the tendon turns under the malleolus, simulates tendinosis but does not produce morphologic alteration (16). Metrics such as the Meary angle and calcaneal inclination are variable in patients with tendinosis but are typically abnormal once the tendon tears (47).

Figure 13. Incomplete PTT tear in a 57-year-old woman. Axial fat-suppressed T2-weighted MR image shows thickening of the PTT (arrow), with fluid-filled clefts in the tendon, indicating intrasubstance degenerative tearing and tenosynovitis. The superomedial band of the spring ligament (arrowhead) separating the PTT from the talus bone, which is rotated internally, is mildly thickened but intact.

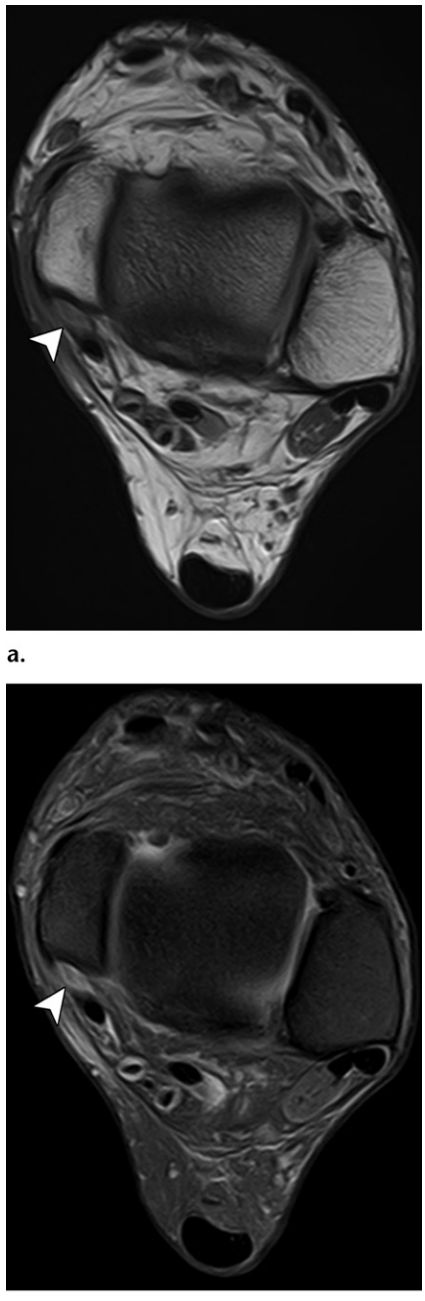

a.

b.

Figure 14. Complete PTT tear in a 52-year-old woman with 4 years of progressive medial ankle pain. Axial T1-weighted **(a)** and fat-suppressed T2-weighted **(b)** MR images show complete absence of the PTT, with a fluid-filled gap at the retromalleolar groove (arrowhead), which is compatible with a type 3 tear. The distal tendon stump (not shown) was retracted and tendinotic. Although complete tears are easily recognized, the distinction between tendinosis and partial tear can be challenging.

Tears are categorized into three types on the basis of tendon caliber and signal intensity; all types may be associated with tenosynovitis and adjacent swelling (44). Type 1 tears are partial thickness intrasubstance tears appearing as linear fluid in a thickened tendon. These interstitial tears are often difficult to distinguish from advanced tendinosis, even at surgical inspection (24) (Fig 13). Types 2 and 3 tears are less common but are more functionally important. Tendon atrophy (smaller than the flexor digitorum longus muscle) indicates a type 2 tear, resulting from fiber loss and tendon attrition (38). The type 3 tear is complete, producing a fluid-filled gap or segmental absence of the tendon (Fig 14). More than 90% of PTT tears involve the retromalleolar or inframalleolar tendon, with inframalleolar tearing (including insertional tearing at the navicular bone attachment) as the most common type (28,42). Supramalleolar tears and diffuse tearing of multiple segments of the tendon are seen less frequently (42).

Accessory Navicular Bone

The accessory navicular bone is a developmental ossicle at the proximal medial navicular bone present in 2%–14% of adults (48). Three types are described: *(a)* Type I is a 2–3-mm sesamoid bone in the PTT, without any cartilaginous connection with the navicular bone; *(b)* type II is connected to the navicular bone tuberosity by a 1–2-mm layer of cartilage; and *(c)* type III is a

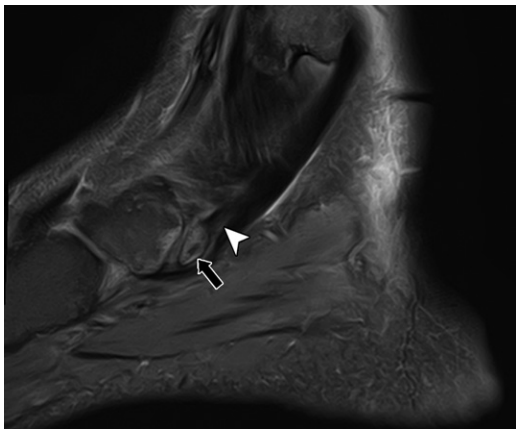

Figure 15. Symptomatic accessory navicular bone in a 39-year-old woman with long-standing focal pain at the medial navicular bone. Sagittal fat-suppressed T2-weighted MR image shows a triangular ossicle (arrow) with its base closely apposed to the navicular bone, which is typical of a type II accessory navicular bone. There is marrow edema in the ossicle and adjacent navicular bone, mild regional inflammation, and altered signal intensity in the terminal fibers of the PTT near its insertion (arrowhead). Note that the PTT inserts predominantly onto the ossicle rather than the more distal navicular bone, altering its mechanics.

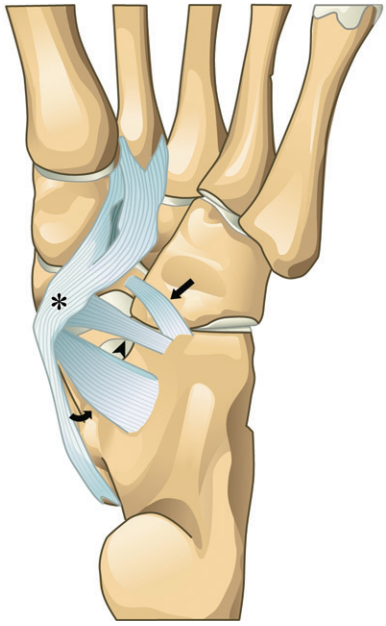

Figure 16. Spring ligament from the plantar perspective. Illustration shows the large superomedial (curved arrow) and smaller medioplantar oblique (arrowhead) and inferoplantar longitudinal (straight arrow) bundles of the spring ligament and their courses as they connect the calcaneus to the navicular bone. The superomedial bundle is most commonly abnormal in patients with AAFD. The medioplantar and inferoplantar bundles were originally considered a single ligament but are now recognized as distinct structures. Note that the plantar fibers of the PTT (*) lie superficial to the medial navicular attachments of the spring ligament, helping to support the ligament.

bulky bone protuberance fused with the navicular bone tuberosity (39,49–51). The majority of accessory navicular bones are asymptomatic, but the type II and III variants can cause midfoot pain and a planovalgus foot, typically manifesting at a younger age than that of patients with PTT degeneration (13,39,50). In these types, the more proximal insertion of the PTT decreases its insertional angle, increasing stress and interfering with mechanics (49,51) (Fig 15). Symptoms are most common with the type II variant and are related to damage and destabilization at the synchondrosis. MRI can show marrow edema and cysts in the fragment and the adjacent navicular bone, fluid in the synchondrosis, overlying swelling, and occasionally, bursa formation (50). Uncommonly, the synchondrosis fractures and separates, either from repetitive stress or superimposed trauma (50).

Secondary Stabilizers

Spring Ligament

The spring ligament, also known as the plantar calcaneonavicular ligament, is considered the primary static stabilizer of the medial arch and is second in importance only to the PTT. With the PTT and deltoid ligament, it forms a soft-tissue confluence at the medial navicular bone that prevents excessive talar head descent (10). In conjunction with the anterior and middle facets of the calcaneus and the navicular bone, it forms a deep socket to articulate with the talus bone, a configuration that has been likened to the hip acetabulum (52). The spring ligament consists of three portions, from medial to lateral: the superomedial, medioplantar oblique, and inferoplantar longitudinal bundles (53,54) (Fig 16). The superomedial bundle, which arises from the superomedial sustentaculum tali and passes below the talus and navicular bone tuberosity before inserting on the superomedial distal navicular bone, is the largest and most important. It forms a hammock-like structure that supports the talar head and talonavicular joint and separates the PTT from the talus bone. A fibrocartilage articular-sided coating allows it to glide smoothly against the talus bone (53,54). Spring ligament injury is most commonly caused by PTT insufficiency, leading to a repetitive exaggerated descent of the talar head, which overloads and damages the superomedial bundle (55). Alterations of the spring ligament are seen in 74%–92% of patients with PTT tears, which makes them the most common secondary abnormalities found in these patients (47,55–58). Acute tears of the spring ligament do occur after severe pronation trauma but are far less common (39).

It is challenging to assess the spring ligament clinically, so imaging is important to its

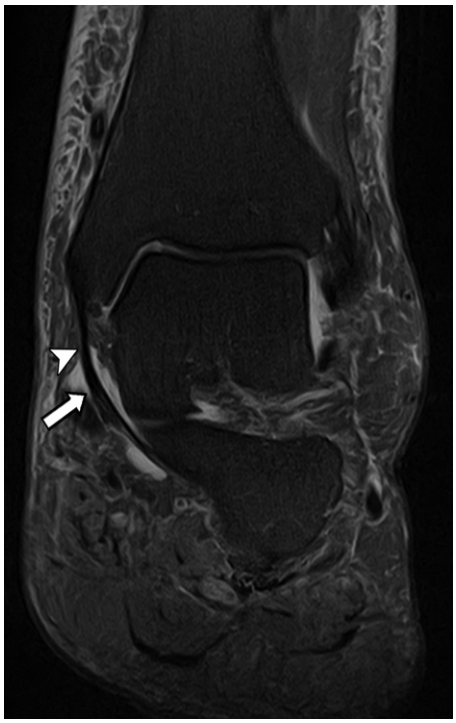

Figure 17. Normal tibiospring ligament in a 45-year-old woman with very mild AAFD. Coronal fat-suppressed proton-density-weighted MR image of the hindfoot shows a normal tibiospring ligament (arrowhead) fusing distally with the superomedial bundle of the spring ligament (arrow), making it the only portion of the deltoid without a distal bone attachment. It is often difficult to tell precisely where these two structures meet, because they form a continuous smooth band that hugs the medial talus bone. This band can be difficult to separate from the overlying PTT unless there is some regional fluid such as that present in this patient.

Figure 18. Spring ligament elongation and degeneration in a 58-year-old woman with advanced AAFD and severe ankle pain. Coronal fat-suppressed T2-weighted MR image of the ankle shows a thickened superomedial spring ligament with heterogeneous signal intensity adjacent to the talar head (thick white arrow), which is consistent with ligament degeneration. There is also ligament elongation caused by repetitive overload by the head of the talus bone as it rotates internally with each foot support maneuver. There is degeneration of the overlying PTT, which is thickened (arrowhead), and alterations of signal intensity at the deltoid ligament (thin arrows) and the sinus tarsi (curved arrow).

Figure 19. Complete tear of the superomedial bundle of the spring ligament in a 67-year-old woman with medial ankle pain with unipodal loading, a palpable bone prominence at the medial midfoot, and the sensation of instability. Coronal fat-suppressed T2-weighted MR image shows the absence of the superomedial bundle of the spring ligament, which should be visible between the talar head (*) and thickened PTT (arrowhead). The plantar components of the spring ligament are thickened, elongated, and irregular (straight arrows). Note the uncovering of the talar head and adjacent soft-tissue edema. Mild inflammatory changes are seen in the tarsal sinus, but the talocalcaneal ligaments appear intact (curved arrows).

evaluation. With US, only the superomedial bundle can be evaluated reliably, and it is best visualized in a sagittal oblique plane parallel to the ligament (59). All components of the spring ligament are well delineated at high-field MRI. The superomedial bundle is best visualized in coronal and axial oblique planes, appearing as a 2–5-mm smooth low-signal-intensity band that is continuous with the superficial deltoid ligament (Fig 17). A spring ligament abnormality is most common at this bundle and typically produces caliber change; ligament thickness greater than 5 mm or less than 2 mm indicates abnormality (54,60) (Fig 18). Additional findings include increased signal intensity, ligament elongation or waviness, fiber discontinuity, and periligamentous edema that typically dominate at the distal ligament (52,57,59). A complete tear allows the PTT to contact the talar head directly, without any intervening tissue (Fig 19). The medioplantar oblique and inferoplantar longitudinal bundles are best seen in

Figure 20. Normal spring ligament recess in an elderly man with symptoms of peroneal tenosynovitis. Axial fat-suppressed proton-density-weighted MR image of the foot shows a normal spring ligament recess (*) interposed between the medioplantar oblique (arrows) and inferoplantar longitudinal (arrowhead) bundles of the spring ligament. The normal recess is well defined, unilocular, and filled with homogeneous fluid. The principal differential diagnosis is a ganglion cyst, which tends to be larger, multilobulated, and septated. Tendinosis and/or the magic angle artifact is present and is causing graying of multiple tendons and the spring ligament. The magic angle artifact can be alleviated by performing MRI sequences with a long echo time at the expense of reduced signal-to-noise ratio.

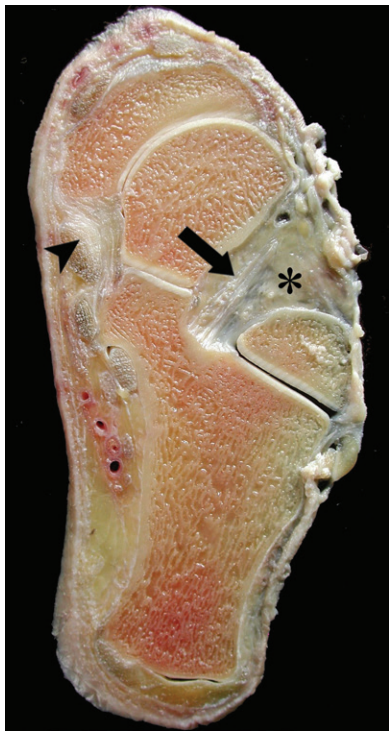

Figure 21. Anatomic specimen of the sinus tarsi. Photograph of an axial slice of the foot shows the sinus tarsi as a conical region of fat (*) flaring open laterally between the talus and calcaneus bones. The interosseous ligament (arrow) is partially visualized. Note the white fibrocartilaginous gliding zone (arrowhead) between the more superficial PTT and the deeper spring ligament just proximal to the navicular bone. In this specimen, the subtalar facets are well aligned. In a patient with AAFD, subtalar instability caused by tearing of the talocalcaneal ligaments leads to translational and rotational malalignment. (Image courtesy of Donald Resnick, MD, University of California, San Diego, Calif.)

the axial plane. An abnormality of these two smaller plantar bundles is less common, more challenging to diagnose, and rarely addressed surgically. The spring ligament recess, which is a normal outpouching of fluid between them, should not be confused with a tear or a ganglion cyst (61) (Fig 20, Table E1).

Sinus Tarsi

The sinus tarsi is a laterally flaring fat-filled conical canal located between the talus and calcaneus bones in front of the posterior subtalar joint. It contains several ligaments that contribute to hindfoot stability (62). Peripherally, bands from the extensor retinaculum enter the sinus tarsi. Anteriorly, the bifurcate ligament connects the midfoot and hindfoot to its calcaneocuboid and calcaneonavicular bands. Centrally, the talocalcaneal ligaments (interosseous and cervical) stabilize the subtalar articulation by limiting talar flexion and rotation relative to the calcaneus (6,62) (Fig 21). Unstable heel valgus leads to repetitive rotation and translation at the subtalar joint, overloading the sinus tarsi ligaments. Talocalcaneal ligament damage produces lateral foot pain and the sensation of hindfoot instability during weight bearing, which is known as sinus tarsi syndrome (55,56,63). In advanced cases, subtalar subluxation with rotation and/or lateral calcaneal drift become apparent.

Sinus tarsi syndrome is difficult to diagnose clinically and shows few radiographic findings. Sonographic assessment is challenging because of the variable depth and orientation of the ligaments and surrounding adipose tissue (62). Alterations of fat signal intensity at MRI are the hallmark of sinus tarsi syndrome (56,63) (Fig 22). The fat may be edematous or fibrotic, depending on the

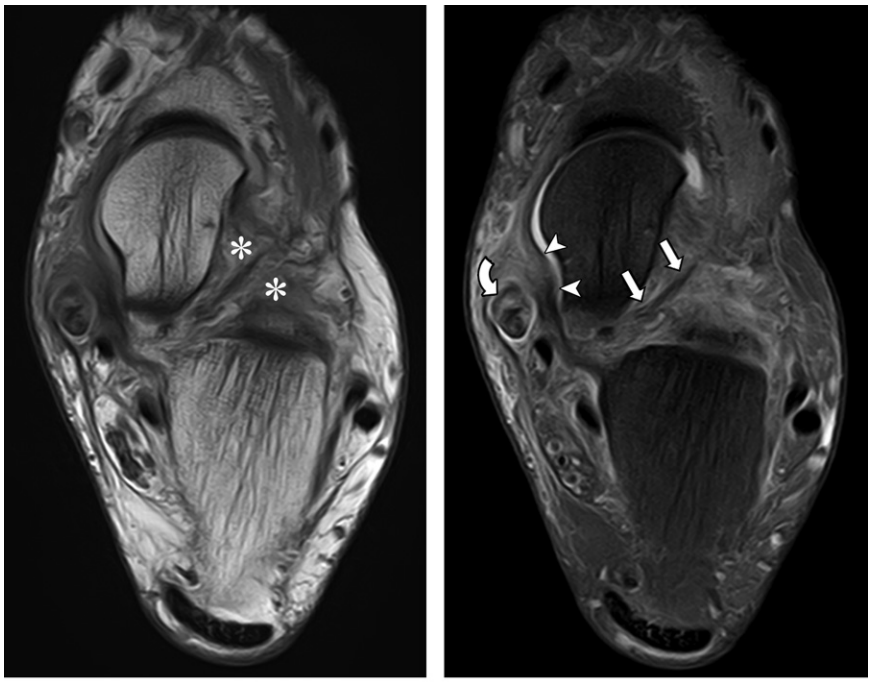

Figure 22. Sinus tarsi syndrome in a 46-year-old woman with pain anterior to the lateral malleolus and a feeling of instability and difficulty walking on unstable surfaces. Axial T1-weighted **(a)** and fat-suppressed proton-density-weighted **(b)** MR images show replacement of the normal sinus tarsi fat (* in **a**) with granulation tissue and fibrosis, with corresponding edema on the fluid-sensitive image. The talocalcaneal ligament appears intact (straight arrows in **b**). The PTT is enlarged with interstitial tearing (curved arrow in **b**) of the tendon, and there is mild tenosynovitis, with thickening of the tendon sheath. The superomedial bundle of the spring ligament lying deep below the PTT is degenerated but still intact (arrowheads in **b**). Note the uncovering of the head of the talus bone that projects medially to the articular surface of the navicular bone.

stage of disease. Additional MRI findings include distortion, tearing, or absence of the talocalcaneal ligaments; synovitis; and soft-tissue and/or intraosseous formation of ganglion cysts (63) (Fig 23). These changes are not pathognomonic of AAFD, because sinus tarsi syndrome also can be caused by acute trauma, chronic ankle instability, and systemic arthropathies (55,63).

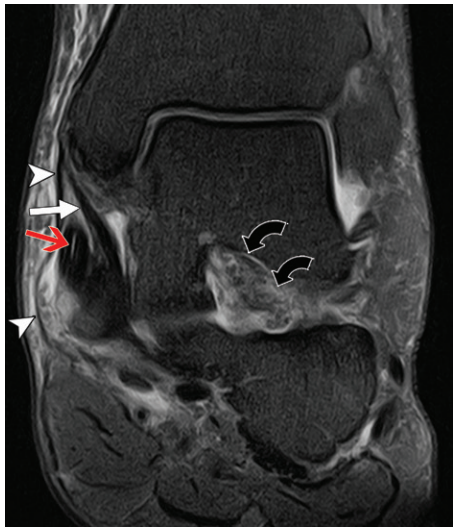

Figure 23. Chronic sinus tarsi syndrome with a talocalcaneal ligament tear and degeneration in a 67-year-old woman with instability aggravated by walking on uneven surfaces. Coronal fat-suppressed proton-density-weighted MR image of the ankle shows edema in the sinus tarsi fat, with thickening, altered signal intensity, and indistinctness of the talocalcaneal ligaments related to degenerative tears (black arrows). There is an intrasubstance split tear of the PTT (red arrow) overlying a thickened superficial deltoid ligament (white arrow) and tenosynovitis of the PTT elevating the flexor retinaculum (arrowheads).

Deltoid Ligament

The deltoid ligament arises from the medial malleolus and consists of deep and superficial layers; anatomic variations in the components of each layer are recognized (64,65). Typically, the deep layer includes an anterior tibiotalar ligament and a more robust posterior tibiotalar ligament; these stabilize the tibiotalar articulation by resisting ankle valgus. The longer superficial deltoid ligaments typically include the tibionavicular and tibiospring ligaments, which span the talonavicular joint, and a tibiocalcaneal ligament, which spans the subtalar joint (66) (Fig 24). The tibionavicular and tibiospring ligaments help to stabilize the talonavicular joint by limiting hindfoot eversion and inward displacement of the talar head, and a deltoid ligament abnormality related to AAFD typically is limited to these structures (17,25,52,55). Damage to the deep deltoid ligament occurs late in the process, allowing the tibiotalar joint to tilt into valgus, aggravating a hindfoot valgus deformity and placing tension on the tibial nerve (25,67).

MRI is the preferred imaging modality for assessment of the deltoid ligament. The axial and coronal planes are most useful for distinguishing its various components, which appear as low- to intermediate-signal-intensity bands that broaden distally (66). Signal intensity becomes heterogeneous as the patient ages, and by itself is not a reliable indicator of ligament abnormality (66).

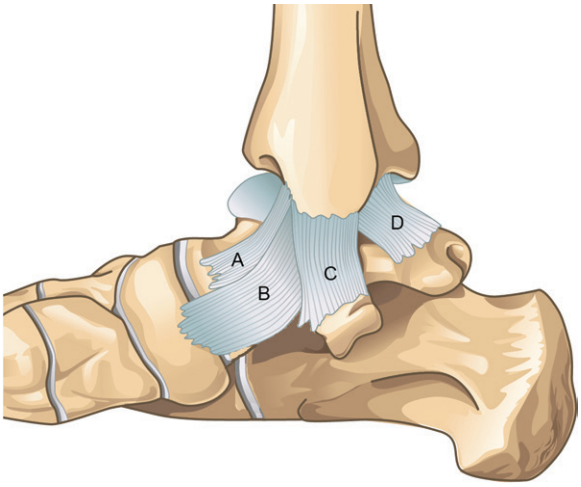

Figure 24. Illustration of the deltoid ligament. The tibionavicular *(A)*, tibiospring *(B)*, and tibiocalcaneal *(C)* components of the superficial deltoid ligament are shown. These ligaments are merged at the medial malleolus and appear as distinct bands only distally. The small deep anterior tibiotalar ligament (not shown) is below the superficial ligaments. The large deep tibiotalar ligament *(D)* is a shorter more robust ligament located posteriorly. The deep deltoid ligaments only cross the ankle joint, whereas the longer superficial ligaments extend further and also cross either the talonavicular joint or subtalar joint.

Figure 25. Torn deep and superficial deltoid ligament in a 55-year-old woman with severe AAFD, lateral pain overlying the tarsal sinus, and medial retromalleolar and subtibial pain. Coronal fat-suppressed proton-density-weighted MR image acquired through the hindfoot shows altered signal intensity and architectural distortion of the posterior bundle of the deep deltoid ligament (arrowhead). In addition, there is linear increased signal intensity in the superficial deltoid ligament related to atraumatic tearing (white straight arrow). The flexor retinaculum is thickened near its medial malleolar insertion (curved arrows), and there is thickening and mild tenosynovitis of the PTT. The spring ligament is attenuated, elongated, and partially torn below the talar head (red arrows). Note the abnormal fat signal intensity related to sinus tarsi syndrome.

Loss of normal fatty striations, signal intensity heterogeneity, and architectural distortion indicate degeneration, low-grade tearing, and fibrosis, whereas high-grade tearing produces large fluid-filled gaps or frank discontinuity (66,68) (Fig 25). High-grade deep deltoid ligament tears are more commonly the result of trauma than they are related to chronic AAFD, which often is associated with concomitant fibular fracture or lateral ligament injury (39,68). Acute injury limited to the deep deltoid ligament does not affect midfoot alignment. Severe injury affecting the superficial ligaments, such as a fascial sleeve injury that avulses the deltoid ligament, tibial periosteum, and flexor retinaculum at the medial malleolus, could cause or exacerbate preexisting midfoot dysfunction (69) (Fig 26).

Plantar Fascia

The plantar fascia is a tough flattened triangular fibrous structure arising from the calcaneal tuberosity that broadens distally to attach at the proximal phalanges. It consists of a thick central cord superficial to the flexor digitorum, a less-prominent lateral cord overlying the abductor digiti minimi, and a small medial cord below the abductor hallucis (70). The plantar fascia is an important support structure that prevents plantar foot elongation and assists in maintaining arch alignment (1,26). Although it is often described as a static stabilizer, it also has a dynamic role during gait through the axis it forms with the Achilles tendon proximally and the plantar plates distally (26,71). Its mechanism of function has been described in several ways. The "truss" concept suggests that a taut fascia functions as the "tie-rod" of a triangular truss formed by the tarsal bones at its two sides and the fascia at the base, minimizing arch descent (11,33). The *windlass mechanism* indicates that the fascia tenses as the toes dorsiflex and the heel elevates during late stance, drawing the heel and metatarsal heads together, thereby shortening the plantar foot and elevating the arch (17,71,72) (Fig 27).

While some consider the plantar fascia to be the most critical structure for arch maintenance, only a modest association between plantar fascia abnormality and flatfoot can be noted with standard imaging. In one study (56), 36% of patients with advanced PTT disease exhibited fascial abnormalities compared with 9% of control subjects, which is an association far weaker than that with spring ligament and sinus tarsi disease. The most common abnormality that affects the plantar fascia is degenerative plantar fasciitis (70).

At US, the degenerated plantar fascia appears thickened and irregular. Elastography demonstrates higher sensitivity than that of conventional

Figure 26. Acute injury of the deltoid ligament complex in a 39-year-old man who was injured playing soccer. **(a)** Coronal T1-weighted image shows a complete tear of the deltoid ligament complex that is wavy and redundant (straight arrows). Portions of the deltoid ligament lie superficial to the PTT (curved arrow), which is the reverse of the normal relationship. There is also a stripping injury of the medial retinaculum (arrowheads) from the medial malleolus. **(b)** Axial T1-weighted image shows the lax irregular retinaculum and superficial deltoid ligament. The normal fatty striations of the deep deltoid fibers are distorted (*).

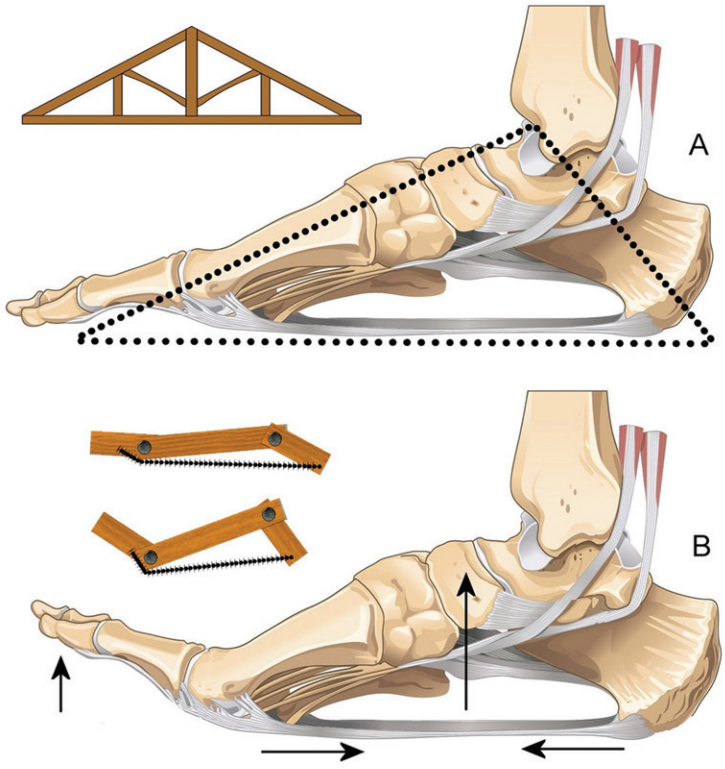

Figure 27. Plantar fascia mechanism of function. *A,* Illustration shows the truss theory, which suggests that the plantar fascia passively prevents elongation of the plantar foot during weight bearing, acting as the "tie-rod" of a triangular structure. In architecture, a truss refers to a rigid framework designed to support a heavy structure such as a roof. *B,* The Hicks windlass theory suggests that the plantar fascia functions dynamically like a winch during toe dorsiflexion, pulling the metatarsal heads and calcaneus closer together to elevate the arch. The term *windlass* refers to a type of winch used for lifting heavy weights by winding a rope or cable around a cylinder.

US, which likely is related to changes in tissue elasticity that are not visible with anatomic imaging (73,74). MRI shows thickening (>4 mm), irregularity, and signal intensity heterogeneity of the fascia at its calcaneal insertion, with variable amounts of perifascial and marrow edema (Fig 28). Superimposed degenerative tears typically affect the central cord near the calcaneus, often after injection of corticosteroids, while traumatic tears occur more distally (70).

Tarsometatarsal Joints

The tarsometatarsal joint forms the midfoot transverse arch that assists in supporting the midfoot during stance and maintaining normal midfoot position for gait (75,76). There are numerous small attachments of the distal PTT at the plantar tarsal and metatarsal surfaces that act in concert with numerous ligaments and capsular structures to maintain tarsometatarsal alignment (77). When these become overloaded, the complex becomes

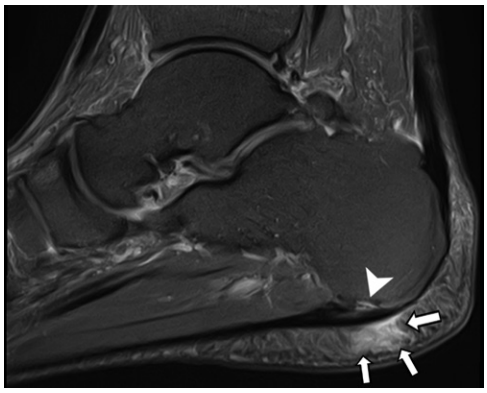

Figure 28. Insertional plantar fasciitis in a 46-year-old woman with AAFD. Sagittal fat-suppressed proton-density-weighted MR image of the heel shows thickening of the central cord and the medial expansion of the plantar fascia at its calcaneal insertion. There is a small focus of altered marrow signal intensity at the enthesis (arrowhead) and overlying plantar fat pad edema (arrows) that is compatible with reactive inflammation. Alignment appears normal on this MR image, although the weight-bearing radiograph (not shown) demonstrated pes planus.

Figure 29. Acute avulsion fracture of the third metatarsal at the PTT insertion in a 35-year-old male soccer player. Axial fat-suppressed proton-density-weighted MR image of the hindfoot shows an undisplaced fracture of the plantar base of the third metatarsal (straight arrow), with one of the small distal insertions of the PTT attached to the fragment (arrowhead). A similar small tendon slip is seen extending to the second metatarsal base, which remains intact (curved arrows). The fracture did not unite and the patient developed painful flattening of the midfoot.

Figure 30. Diabetic neuroarthropathy with midfoot collapse. Lateral radiograph of the weight-bearing foot shows plantar migration of the midfoot with tarsometatarsal collapse. Note the depression of the fragmented distal end of the medial cuneiform bone (*), which is now weight bearing. Because of medial arch failure, the navicular bone is sagging and covering the cuboid bone, and the talus bone is no longer aligned with the first metatarsal. There are screws from a first tarsometatarsal arthrodesis (Lapidus procedure) that was unsuccessful in stabilizing the tarsometatarsal joint.

dysfunctional, leading to transverse arch flattening (55). PTT dysfunction also allows the unopposed peroneus brevis to excessively rotate the forefoot externally, slowly leading to tarsometatarsal malalignment. Although tarsometatarsal malalignment and arthrosis are recognized features of AAFD, imaging of the small distal slips of the PTT and regional ligaments at this region can be challenging unless there is acute injury (Fig 29).

Although AAFD ultimately affects the tarsometatarsal joint, three conditions more commonly associated with primarily transverse arch collapse are primary osteoarthrosis, Lisfranc fracture-dislocation, and neuroarthropathy (3,17). Osteoarthrosis is typically maximal at the second tarsometatarsal joint, which is recessed and stabilizes this region (17). The Lisfranc fracture dislocation affects the same articulation and is overlooked in up to 20% of patients, leading to instability, damage to the plantar supporting structures, and planovalgus deformity (75,76). Neuropathic destruction of the midfoot also can lead to progressive tarsometatarsal collapse, culminating in a "rocker bottom foot," that is prone to ulceration and osteomyelitis (78,79) (Fig 30). The most common cause is diabetes, and the tarsometatarsal articulation is the most commonly affected site (79).

Staging and Treatment of AAFD

The management of AAFD requires consideration of symptoms and physical examination findings; these determine the stage of disease, which in conjunction with imaging findings, guides appropriate treatment. Staging is primarily based on objective findings (the presence or absence of deformity, whether deformity is flexible or rigid, the presence or absence of secondary osteoarthrosis) rather than symptoms. Symptom severity does not always correlate with the extent of deformity, possibly because preexisting flatfoot emphasizes malalignment or the cessation of inflammation after

Table 3: AAFD Staging and Treatment (Simplified Bluman-Myerson Classification)

Stage	Deformity	Disease Progression	Treatment
I	None	PTT tendinosis or tenosynovitis Functional tendon	Conservative treatment initially Tenosynovectomy
II			
IIA	Flexible moderate deformity (<40% of the talar head uncovered)	Tendinosis or a low- to moderate-grade tear of the PTT Laxity of the spring ligament	Orthoses Tendon transfer Medializing calcaneal osteotomy Subtalar arthroereisis Medial column stabilizing procedure
IIB	Flexible severe deformity (>40% of the talar head uncovered or subtalar impingement)	High-grade tear of PTT Incompetent spring ligament Sinus tarsi syndrome	Consider adding lateral column lengthening with or without spring ligament reconstruction
III	Rigid (inflexible) deformity	Subtalar osteoarthrosis Lateral hindfoot impingement	Subtalar arthrodesis or triple arthrodesis Consider adding medial ray procedure for plantar flexion of the first metatarsal
IV			
IVA	Flexible tibiotalar valgus	Deltoid ligament abnormality	Flatfoot reconstruction and deltoid ligament reconstruction
IVB	Rigid tibiotalar valgus	Tibiotalar osteoarthrosis	Consider adding tibiotalar fusion or ankle arthroplasty

complete tendon rupture mitigates pain (36,40). All commonly used staging systems are based on the seminal work by Johnson and Strom (80), who described three stages of dysfunction. The widely used Myerson staging system is an expanded modification of this original system and describes four stages of disease, various substages, and treatment recommendations (5,37,67,80) (Table 3). As with all categorization systems, there can be difficulty in differentiating between adjacent stages, because the underlying abnormality develops along a continuum (4).

Stage I

In stage I AAFD, symptoms include posteromedial ankle pain, tenderness along the course of the PTT, and decreased endurance. Swelling may be prominent in patients with tenosynovitis, but tendon length is normal, and the alignment and function of the foot are preserved (37). Treatment is generally conservative, consisting of nonsteroidal anti-inflammatory medications, local corticosteroid and/or anesthetic injections, and physical therapy (16). Tenosynovectomy may be needed for recalcitrant disease (17).

Stage II

In stage II disease, flexible deformity develops, resulting in clinically apparent diminished space below the arch while weight bearing. Functionally, there is weakness of inversion of the plantarflexed foot and an inability to perform a single-leg heel rise. The test is performed by having the patient stand on his or her toes, first on both feet and then on a single foot. Normally, the heel swings into varus position as it rises; when the PTT is insufficient, the heel fails to invert or the patient is unable to perform the maneuver (17). Unlike physiologic flatfoot, rotational deformity of the hindfoot and heel valgus may be apparent, although it is mild in early stage II disease (3,17) (Fig 31). Malalignment produces the "too many

Figure 31. Typical foot deformity in a 52-year-old man with unilateral AAFD. Clinical photograph shows flattening of the medial arch of the right foot, which is associated with mild heel valgus and external rotation of the foot. The normal left foot serves as a useful comparison and highlights the peritalar pattern of malalignment typical of AAFD. (Image courtesy of Rosa Pinto Camacho, MD, Camacho Podoclinic, Medellín, Colombia.)

Figure 32. "Too many toes" sign in a 35-year-old man with AAFD for 10 years. Clinical photograph shows that when viewed from the back during weight bearing, three lateral toes are clearly visible from behind the patient's left foot, whereas only the fifth toe is visible behind the normal right foot. Note the pes planus and mild heel valgus deformity in the left foot, with the calcaneus tilted into valgus relative to the tibial axis, resulting in prominence of the medial midfoot. (Image courtesy of Rosa Pinto Camacho, MD, Camacho Podoclinic, Medellín, Colombia.)

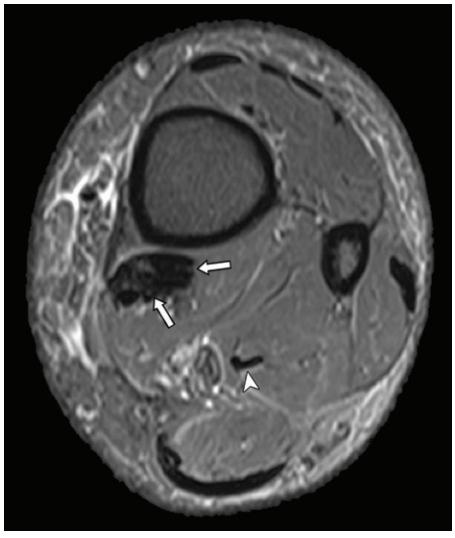

Figure 33. Tendon transfer for PTT insufficiency in a 54-year-old woman with Stage II AAFD after side-to-side fixation of the flexor digitorum longus and posterior tibialis tendons. Axial fat-suppressed proton-density-weighted MR image shows a markedly thickened tendon at their confluence (arrows). This normal postoperative appearance should not be confused with tendinosis and tearing of the PTT. Note the normal flexor hallucis longus tendon (arrowhead) located posterolateral to the reconstruction. Complications of tendon transfer include excessive tension at the reconstruction and a weakened heel rise.

toes" sign, which refers to visualization of more than one of the lateral toes when viewing the foot from behind during weight bearing owing to heel valgus (17,36,80) (Fig 32).

Orthoses limiting forefoot pronation or a walker boot restricting all ankle movement allow the PTT to rest and heal and may be sufficient in patients with mild stage II disease (16). Patients with advanced stage II disease typically are treated surgically. Procedures are classified into those that address the soft tissue, the bone, or both. Posterior tibial tendon débridement and reattachment are options only if the native tendon is functional and salvageable. Tendon transfers with the use of the flexor hallucis longus or flexor digitorum longus tendon are the staples of soft-tissue repair (16). The transferred tendon can work along with a diseased PTT or can replace one that is completely torn (81) (Fig 33). Other soft-tissue procedures include augmentation of the spring ligament and lengthening of the Achilles tendon (81–83).

Medializing calcaneal osteotomy is widely used for treatment of AAFD, either alone, or more commonly, in conjunction with other soft-tissue or bone procedures (Fig 34). Medializing the calcaneal tuberosity restores Achilles alignment medial to the subtalar axis, allowing it to function as a hindfoot inverter, relieving strain on the native or reconstructed medial structures (35,81,83). Subtalar hyperpronation can be addressed with placement of a subtalar implant (subtalar arthroereisis), a procedure that was developed originally for pediatric patients but currently also is used in adults (84) (Fig 35). Medial column stabilizing surgery performed to fuse part of or the entire medial column becomes necessary when the talus bone is substantially uncovered. Commonly used procedures include talonavicular, navicular-cuneiform, and/or first tarsometatarsal arthrodesis (Lapidus procedure) (3,4). Fixed dorsiflexion of the first ray that interferes with re-creation of the medial arch can be remedied with an opening wedge osteotomy (Cotton osteotomy) (16).

Stage III

In stage III disease, the deformities found in stage II disease become irreducible even with manipulation, and the foot becomes inflexible, leading to secondary midfoot arthrosis (16,80). Fixed hindfoot valgus and lateral column shortening at this stage often result in symptoms shifting from the medial to the lateral foot as the patient develops lateral hindfoot impingement (36). Impingement correlates with deterioration of the hindfoot valgus angle and can affect the talocalcaneal joint, subfibular region, or both regions simultaneously (23). Talocalcaneal impingement causes pain and osseous changes of edema, cysts, and sclerosis where the lateral talar process impacts the calcaneus (Fig 36).

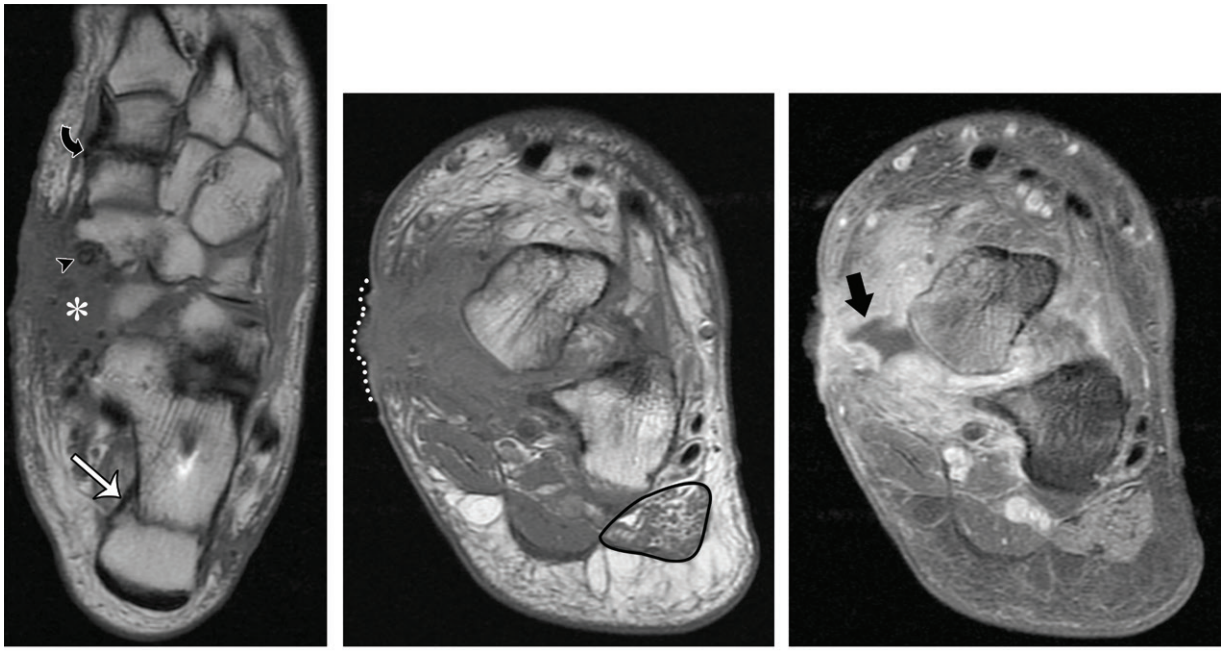

a. b. c.

Figure 34. Postoperative infection in a 36-year-old man. **(a)** Axial T1-weighted MR image obtained after medializing calcaneal osteotomy (white arrow), medial cuneiform osteotomy (black arrow) and navicular anchor for soft-tissue reconstruction (arrowhead) shows extensive soft tissue at the medial foot (∗) with loss of all normal soft-tissue structures. **(b)** Coronal T1-weighted MR image shows soft-tissue thickening at the surgical bed, with skin irregularity (dotted line) overlying the talar head, which shows subtle marrow alterations. Note the atrophy of the abductor digiti minimi muscle (outlined in black), which suggests denervation myopathy and is seen commonly in patients with advanced AAFD with plantar fascia degeneration. **(c)** Coronal contrast material–enhanced fat-suppressed T1-weighted MR image shows avid enhancement of the bone and soft tissues, with a nonenhancing collection of fluid (arrow) that was draining at the skin medial to the talar head.

Figure 35. Arthroereisis and osteotomy of the medial cuneiform in a 22-year-old man with stage II AAFD. Postoperative lateral radiograph of the weight-bearing foot shows an arthroereisis implant placed in the subtalar space (arrow) to elevate the midfoot and prevent pronation of the talus bone, thereby limiting excessive hindfoot valgus. In young patients, arthroereisis generally is preferred over subtalar arthrodesis because it preserves some joint motion. Complications include sinus tarsi pain and implant migration. Two screws are seen at the medial cuneiform opening wedge osteotomy (Cotton osteotomy), which was performed to assist in plantar flexion of the first ray.

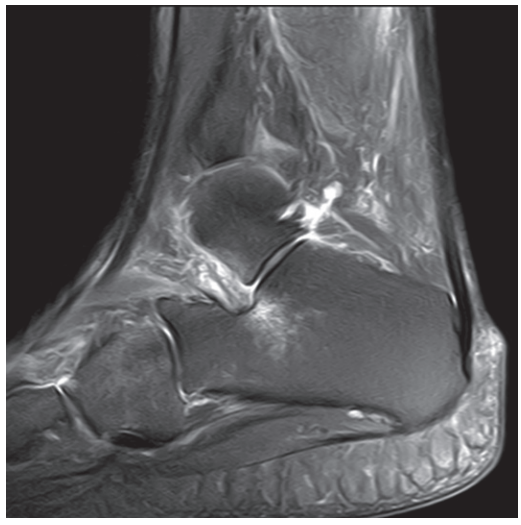

Figure 36. Hindfoot valgus leading to talocalcaneal impingement in a 68-year-old woman. Sagittal fat-suppressed proton-density-weighted sagittal MR image shows bone marrow edema in the calcaneus below the angle of Gissane. The process of talocalcaneal impingement occurs because of repetitive pressure from the lateral talar process and often is associated with peritalar instability and sinus tarsi syndrome. As talocalcaneal impingement advances, bone sclerosis and cystic changes develop at both the talus and the calcaneus bones. Note the mild edema at the cuboid bone, which also is related to lateral foot overload.

Subfibular impingement produces similar bone findings between the distal fibula and lateral calcaneal wall and can be associated with soft-tissue fibrosis, bursa formation, and calcaneofibular ligament and peroneal tendon entrapment (23) (Fig 37). In extreme cases, altered weight bearing leads to an insufficiency fracture; these occur most commonly at the distal fibula, although other locations are described (85).

It is not uncommon that adults are first diagnosed with congenital tarsal coalition while they

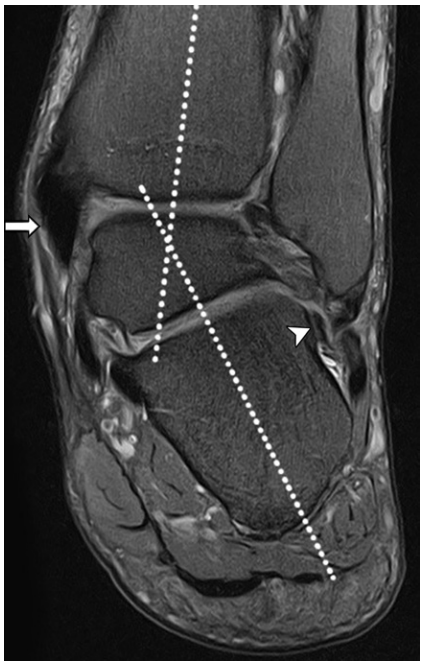

Figure 37. Subfibular impingement in a 64-year-old woman with lateral submalleolar pain. Coronal fat-suppressed proton-density-weighted MR image shows crowding of the peroneal tendons and the calcaneofibular ligament (arrowhead) due to narrowing of the space between the fibula and lateral calcaneal wall. With chronic impingement, these soft-tissue structures can degenerate and tear. Note the valgus deformity of the hindfoot with the calcaneus tilted laterally relative to the tibial axis (dotted lines). A thickened PTT is seen in the long axis behind the medial malleolus (arrow).

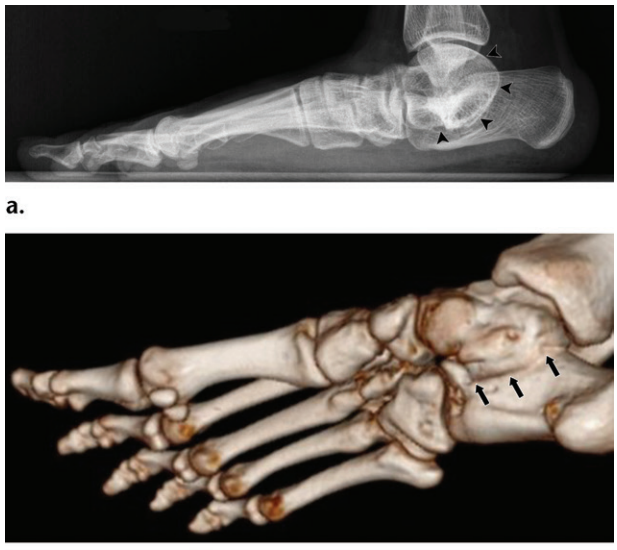

a.

b.

Figure 38. Subtalar coalition manifesting as a rigid flatfoot deformity in a 23-year-old woman. **(a)** Lateral radiograph of the left foot shows malalignment with loss of calcaneal inclination. The classic "C sign" of a subtalar coalition (arrowheads) can be seen. **(b)** Oblique three-dimensional CT reconstruction shows the inferomedial foot from below and allows confirmation of the presence of an osseous coalition at the medial subtalar facet (arrows). The patient's right foot was normal. She underwent surgical reconstruction.

are undergoing imaging for stage III AAFD, because the altered foot shape in coalition with arch flattening and rigid hindfoot valgus is similar. The estimated incidence of coalition is 1%–2% of the population and the condition is bilateral in 50%–60% of those with coalition (2,86,87). Medial subtalar facet and calcaneonavicular coalition occur with equal frequency; these two forms make up 90% of all tarsal coalitions (87). Radiography, CT, and MRI allow diagnosis and assessment of the type of coalition, the extent of fusion, and the associated soft-tissue abnormalities (Fig 38).

In stage III disease, lateral column-lengthening procedures may be needed in conjunction with medial stabilization to address heel valgus and forefoot abduction. These procedures derotate the hindfoot out of valgus, realigning the foot and relieving lateral impingement (16,17). Lengthening is accomplished through either an opening calcaneal osteotomy with bone graft augmentation or calcaneocuboid distraction arthrodesis. Triple arthrodesis, which fuses the subtalar, talonavicular, and calcaneocuboid articulations, is used when the joints are severely degenerated but causes rigidity and can be complicated by malunion, nonunion, and talar dome necrosis (17,83) (Fig 39).

Stage IV

Stage IV disease mandates involvement of the tibiotalar joint. This stage develops when the deep deltoid ligament is incompetent and the tibiotalar joint drifts into valgus, aggravating lateral hindfoot impingement and leading to concomitant tibiotalar instability and arthrosis (Fig 40). Symptoms at this stage often shift from the foot to the ankle joint. Deltoid ligament reconstruction, in addition to the flatfoot realignment procedures already described, is used while the ankle joint is still flexible (67,88). If the tibiotalar joint is fixed in valgus or has substantial arthritis, tibiotalar fusion may be necessary.

Conclusion

AAFD most commonly is caused by a cascade of abnormalities in the foot that start with PTT dysfunction and ultimately lead to damage of other supporting soft tissue, malalignment, gait abnormality, and arthrosis. This article has outlined the relevant anatomy, biomechanics, pathophysiology, imaging findings, and management strategies associated with AAFD. We hope it helps radiologists by enhancing their understanding of foot alignment, function, and

Figure 39. Triple arthrodesis in a 62-year-old woman with stage III AAFD and secondary arthrosis. Anteroposterior radiograph of the weight-bearing foot shows medial column stabilization performed by fusing the talonavicular joint with two screws and lateral column stabilization and fusion with a calcaneocuboid plate. The longer screw at the midfoot is placed for subtalar arthrodesis. Complete rupture of the PTT was confirmed intraoperatively.

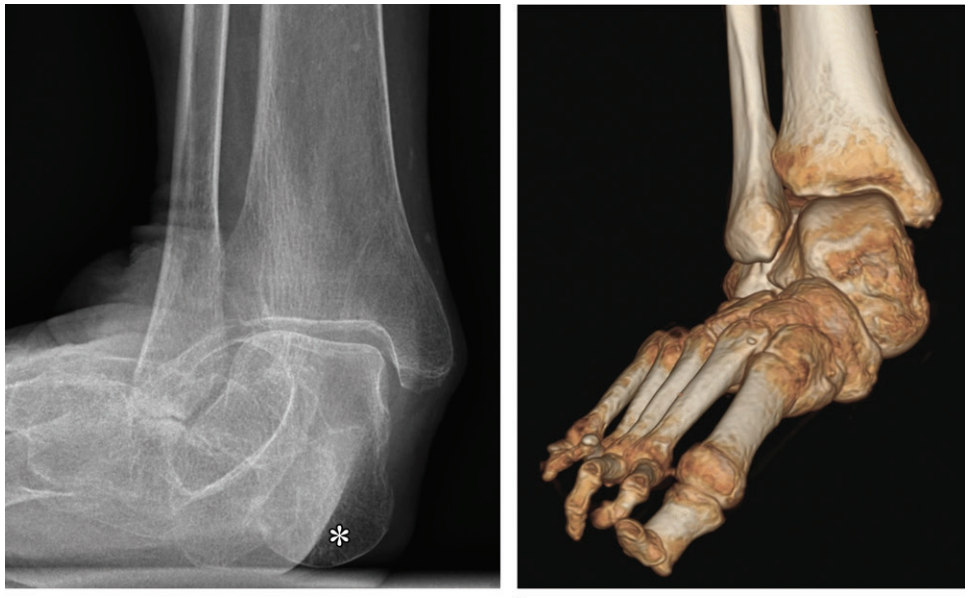

a. **b.**

Figure 40. Stage IV AAFD with involvement of the tibiotalar joint in an elderly woman. **(a)** Anteroposterior radiograph of the weight-bearing ankle shows tibiotalar valgus with narrowing of the superolateral ankle joint, which indicates deltoid ligament dysfunction. There is hindfoot valgus with gross talar uncovering, and the talus bone is almost vertical with its talar head (*) resting at the ground. **(b)** Corresponding three-dimensional CT image shows the advanced malalignment of long-standing AAFD with talar drooping and external rotation of the foot that uncovers the talar head. Note that the tibiotalar disease is less apparent when the foot is not bearing weight. Three-dimensional CT is helpful for the surgeon to identify the joints that are most unstable and plan the complex surgical procedures necessary to manage this degree of foot malalignment.

dysfunction and by increasing their awareness of the imaging appearance of this disabling disorder.

Acknowledgment.—The authors give special thanks to Judy Ann D. Tamayo, Quezon City, the Philippines, for preparing the graphic illustrations.

References

1. Van Boerum DH, Sangeorzan BJ. Biomechanics and pathophysiology of flat foot. Foot Ankle Clin 2003;8(3):419–430.
2. Harris EJ, Vanore JV, Thomas JL, et al. Diagnosis and treatment of pediatric flatfoot. J Foot Ankle Surg 2004;43(6):341–373.
3. Lee MS, Vanore JV, Thomas JL, et al. Diagnosis and treatment of adult flatfoot. J Foot Ankle Surg 2005;44(2):78–113.
4. Pinney SJ, Lin SS. Current concept review: acquired adult flatfoot deformity. Foot Ankle Int 2006;27(1):66–75.
5. Guelfi M, Pantalone A, Mirapeix RM, et al. Anatomy, pathophysiology and classification of posterior tibial tendon dysfunction. Eur Rev Med Pharmacol Sci 2017;21(1): 13–19.
6. Riegger CL. Anatomy of the ankle and foot. Phys Ther 1988;68(12):1802–1814.
7. McKeon PO, Hertel J, Bramble D, Davis I. The foot core system: a new paradigm for understanding intrinsic foot muscle function. Br J Sports Med 2015;49(5):290.
8. Gwani AS, Asari MA, Mohd Ismail ZI. How the three arches of the foot intercorrelate. Folia Morphol (Warsz) 2017;76(4):682–688.
9. Karasick D, Schweitzer ME. Tear of the posterior tibial tendon causing asymmetric flatfoot: radiologic findings. AJR Am J Roentgenol 1993;161(6):1237–1240.
10. Gray H. Arthrology. In: Anatomy of the Human Body. 37th ed. Edinburgh, Scotland: Churchill Livingstone, 1989; 542–544.
11. Richie DH Jr. Biomechanics and clinical analysis of the adult acquired flatfoot. Clin Podiatr Med Surg 2007;24(4):617–644, vii.
12. Uden H, Scharfbillig R, Causby R. The typically developing paediatric foot: how flat should it be? A systematic review. J Foot Ankle Res 2017;10(1):37.
13. Popko J, Guszczyn T, Kwiatkowski M, Komarnicki B. Pediatric flat feet. Pol J Appl Sci 2017;3(1):20–25.
14. Carr JB 2nd, Yang S, Lather LA. Pediatric Pes Planus: A State-of-the-Art Review. Pediatrics 2016;137(3):e20151230.
15. Gould N, Moreland M, Alvarez R, Trevino S, Fenwick J. Development of the child's arch. Foot Ankle 1989;9 (5):241–245.
16. Ling SK, Lui TH. Posterior Tibial Tendon Dysfunction: An Overview. Open Orthop J 2017;11:714–723.
17. Lever CJ, Hennessy MS. Adult flat foot deformity. Orthop Trauma 2016;30(1):41–50.
18. Lamm BM, Stasko PA, Gesheff MG, Bhave A. Normal Foot and Ankle Radiographic Angles, Measurements, and Reference Points. J Foot Ankle Surg 2016;55(5):991–998.
19. Gentili A, Masih S, Yao L, Seeger LL. Pictorial review: foot axes and angles. Br J Radiol 1996;69(826):968–974.
20. Oestreich AE. How to Measure Angles from Foot Radiographs: A Primer. New York, NY: Springer-Verlag, 1990.
21. Williamson ER, Chan JY, Burket JC, Deland JT, Ellis SJ. New radiographic parameter assessing hindfoot alignment in stage II adult-acquired flatfoot deformity. Foot Ankle Int 2015;36(4):417–423.
22. Reilingh ML, Beimers L, Tuijthof GJM, Stufkens SA, Maas M, van Dijk CN. Measuring hindfoot alignment radiographically: the long axial view is more reliable than the hindfoot alignment view. Skeletal Radiol 2010;39(11):1103–1108.
23. Donovan A, Rosenberg ZS. Extraarticular lateral hindfoot impingement with posterior tibial tendon tear: MRI correlation. AJR Am J Roentgenol 2009;193(3):672–678.
24. Conti S, Michelson J, Jahss M. Clinical significance of magnetic resonance imaging in preoperative planning for reconstruction of posterior tibial tendon ruptures. Foot Ankle 1992;13(4):208–214.
25. Ormsby N, Jackson G, Evans P, Platt S. Imaging of the Tibionavicular Ligament, and Its Potential Role in Adult Acquired Flatfoot Deformity. Foot Ankle Int 2018;39(5):629–635.
26. Cifuentes-De la Portilla C, Larrainzar-Garijo R, Bayod J. Biomechanical stress analysis of the main soft tissues associated with the development of adult acquired flatfoot deformity. Clin Biomech (Bristol, Avon) 2019;61: 163–171.
27. Imhauser CW, Siegler S, Abidi NA, Frankel DZ. The effect of posterior tibialis tendon dysfunction on the plantar pressure characteristics and the kinematics of the arch and the hindfoot. Clin Biomech (Bristol, Avon) 2004;19(2):161–169.
28. Chhabra A, Soldatos T, Chalian M, et al. 3-Tesla magnetic resonance imaging evaluation of posterior tibial tendon dysfunction with relevance to clinical staging. J Foot Ankle Surg 2011;50(3):320–328.
29. Arnoldner MA, Gruber M, Syré S, et al. Imaging of posterior tibial tendon dysfunction--Comparison of high-resolution ultrasound and 3T MRI. Eur J Radiol 2015;84(9):1777–1781.
30. Schweitzer ME, Karasick D. MR imaging of disorders of the posterior tibialis tendon. AJR Am J Roentgenol 2000;175(3):627–635.
31. Manske MC, McKeon KE, Johnson JE, McCormick JJ, Klein SE. Arterial anatomy of the tibialis posterior tendon. Foot Ankle Int 2015;36(4):436–443.
32. Bloome DM, Marymont JV, Varner KE. Variations on the insertion of the posterior tibialis tendon: a cadaveric study. Foot Ankle Int 2003;24(10):780–783.
33. Walters JL, Mendicino SS. The flexible adult flatfoot: anatomy and pathomechanics. Clin Podiatr Med Surg 2014;31(3):329–336.
34. Ness ME, Long J, Marks R, Harris G. Foot and ankle kinematics in patients with posterior tibial tendon dysfunction. Gait Posture 2008;27(2):331–339.
35. Brodsky JW. Preliminary gait analysis results after posterior tibial tendon reconstruction: a prospective study. Foot Ankle Int 2004;25(2):96–100.
36. Vulcano E, Deland JT, Ellis SJ. Approach and treatment of the adult acquired flatfoot deformity. Curr Rev Musculoskelet Med 2013;6(4):294–303.
37. Abousayed MM, Tartaglione JP, Rosenbaum AJ, Dipreta JA. Classifications in Brief: Johnson and Strom Classification of Adult-acquired Flatfoot Deformity. Clin Orthop Relat Res 2016;474(2):588–593.
38. Kong A, Van Der Vliet A. Imaging of tibialis posterior dysfunction. Br J Radiol 2008;81(970):826–836.
39. Ribbans WJ, Garde A. Tibialis posterior tendon and deltoid and spring ligament injuries in the elite athlete. Foot Ankle Clin 2013;18(2):255–291.
40. Khoury NJ, el-Khoury GY, Saltzman CL, Brandser EA. MR imaging of posterior tibial tendon dysfunction. AJR Am J Roentgenol 1996;167(3):675–682.
41. Lim PS, Schweitzer ME, Deely DM, et al. Posterior tibial tendon dysfunction: secondary MR signs. Foot Ankle Int 1997;18(10):658–663.
42. Jain NB, Omar I, Kelikian AS, van Holsbeeck L, Grant TH. Prevalence of and factors associated with posterior tibial tendon pathology on sonographic assessment. PM R 2011;3(11):998–1004.
43. Fessell DP, Vanderschueren GM, Jacobson JA, et al. US of the ankle: technique, anatomy, and diagnosis of pathologic conditions. RadioGraphics 1998;18(2):325–340.
44. Rosenberg ZS, Cheung Y, Jahss MH, Noto AM, Norman A, Leeds NE. Rupture of posterior tibial tendon: CT and MR imaging with surgical correlation. Radiology 1988;169(1):229–235.
45. Premkumar A, Perry MB, Dwyer AJ, et al. Sonography and MR imaging of posterior tibial tendinopathy. AJR Am J Roentgenol 2002;178(1):223–232.
46. Delfaut EM, Demondion X, Bieganski A, Cotten H, Mestdagh H, Cotten A. The fibrocartilaginous sesamoid: a cause of size and signal variation in the normal distal posterior tibial tendon. Eur Radiol 2003;13(12):2642–2649.
47. Lin YC, Mhuircheartaigh JN, Lamb J, Kung JW, Yablon CM, Wu JS. Imaging of adult flatfoot: correlation of radiographic measurements with MRI. AJR Am J Roentgenol 2015;204(2):354–359.

48. Knapik DM, Guraya SS, Conry KT, Cooperman DR, Liu RW. Longitudinal radiographic behavior of accessory navicular in pediatric patients. J Child Orthop 2016;10(6):685–689.
49. Bernaerts A, Vanhoenacker FM, Van de Perre S, De Schepper AM, Parizel PM. Accessory navicular bone: not such a normal variant. JBR-BTR 2004;87(5):250–252.
50. Miller TT, Staron RB, Feldman F, Parisien M, Glucksman WJ, Gandolfo LH. The symptomatic accessory tarsal navicular bone: assessment with MR imaging. Radiology 1995;195(3):849–853.
51. Choi YS, Lee KT, Kang HS, Kim EK. MR imaging findings of painful type II accessory navicular bone: correlation with surgical and pathologic studies. Korean J Radiol 2004;5(4):274–279.
52. Omar H, Saini V, Wadhwa V, Liu G, Chhabra A. Spring ligament complex: Illustrated normal anatomy and spectrum of pathologies on 3T MR imaging. Eur J Radiol 2016;85(11):2133–2143.
53. Taniguchi A, Tanaka Y, Takakura Y, Kadono K, Maeda M, Yamamoto H. Anatomy of the spring ligament. J Bone Joint Surg Am 2003;85(11):2174–2178.
54. Mengiardi B, Zanetti M, Schöttle PB, et al. Spring ligament complex: MR imaging-anatomic correlation and findings in asymptomatic subjects. Radiology 2005;237(1):242–249.
55. Deland JT, de Asla RJ, Sung IH, Ernberg LA, Potter HG. Posterior tibial tendon insufficiency: which ligaments are involved? Foot Ankle Int 2005;26(6):427–435.
56. Balen PF, Helms CA. Association of posterior tibial tendon injury with spring ligament injury, sinus tarsi abnormality, and plantar fasciitis on MR imaging. AJR Am J Roentgenol 2001;176(5):1137–1143.
57. Toye LR, Helms CA, Hoffman BD, Easley M, Nunley JA. MRI of spring ligament tears. AJR Am J Roentgenol 2005;184(5):1475–1480.
58. Rule J, Yao L, Seeger LL. Spring ligament of the ankle: normal MR anatomy. AJR Am J Roentgenol 1993;161(6):1241–1244.
59. Mansour R, Teh J, Sharp RJ, Ostlere S. Ultrasound assessment of the spring ligament complex. Eur Radiol 2008;18(11):2670–2675.
60. Yao L, Gentili A, Cracchiolo A. MR imaging findings in spring ligament insufficiency. Skeletal Radiol 1999;28(5):245–250.
61. Desai KR, Beltran LS, Bencardino JT, Rosenberg ZS, Petchprapa C, Steiner G. The spring ligament recess of the talocalcaneonavicular joint: depiction on MR images with cadaveric and histologic correlation. AJR Am J Roentgenol 2011;196(5):1145–1150.
62. Stella SM, Ciampi B, Orsitto E, Melchiorre D, Lippolis PV. Sonographic visibility of the sinus tarsi with a 12 MHz transducer. J Ultrasound 2014;19(2):107–113.
63. Lektrakul N, Chung CB, Lai Ym, et al. Tarsal sinus: arthrographic, MR imaging, MR arthrographic, and pathologic findings in cadavers and retrospective study data in patients with sinus tarsi syndrome. Radiology 2001;219(3):802–810.
64. Milner CE, Soames RW. The medial collateral ligaments of the human ankle joint: anatomical variations. Foot Ankle Int 1998;19(5):289–292.
65. Boss AP, Hintermann B. Anatomical study of the medial ankle ligament complex. Foot Ankle Int 2002;23(6):547–553.
66. Mengiardi B, Pfirrmann CW, Vienne P, Hodler J, Zanetti M. Medial collateral ligament complex of the ankle: MR appearance in asymptomatic subjects. Radiology 2007;242(3):817–824.
67. Bluman EM, Title CI, Myerson MS. Posterior tibial tendon rupture: a refined classification system. Foot Ankle Clin 2007;12(2):233–249, v.
68. Chhabra A, Subhawong TK, Carrino JA. MR imaging of deltoid ligament pathologic findings and associated impingement syndromes. RadioGraphics 2010;30(3):751–761.
69. Crim J, Longenecker LG. MRI and surgical findings in deltoid ligament tears. AJR Am J Roentgenol 2015;204(1):W63–W69.
70. Theodorou DJ, Theodorou SJ, Kakitsubata Y, et al. Plantar fasciitis and fascial rupture: MR imaging findings in 26 patients supplemented with anatomic data in cadavers. RadioGraphics 2000;20(Spec No):S181–S197.
71. Caravaggi P, Pataky T, Goulermas JY, Savage R, Crompton R. A dynamic model of the windlass mechanism of the foot: evidence for early stance phase preloading of the plantar aponeurosis. J Exp Biol 2009;212(Pt 15):2491–2499.
72. Hicks JH. The mechanics of the foot. II. The plantar aponeurosis and the arch. J Anat 1954;88(1):25–30.
73. Sconfienza LM, Silvestri E, Orlandi D, et al. Real-time sonoelastography of the plantar fascia: comparison between patients with plantar fasciitis and healthy control subjects. Radiology 2013;267(1):195–200.
74. Taljanovic MS, Gimber LH, Becker GW, et al. Shear-Wave Elastography: Basic Physics and Musculoskeletal Applications. RadioGraphics 2017;37(3):855–870.
75. Siddiqui NA, Galizia MS, Almusa E, Omar IM. Evaluation of the tarsometatarsal joint using conventional radiography, CT, and MR imaging. RadioGraphics 2014;34(2):514–531.
76. Pietsch E. Injuries to the Lisfranc Joint and its Significance for the Patient. EC Orthop 2017;5(6):246–254. https://www.ecronicon.com/ecor/pdf/ECOR-05-00149.pdf.
77. Castro M, Melão L, Canella C, et al. Lisfranc joint ligamentous complex: MRI with anatomic correlation in cadavers. AJR Am J Roentgenol 2010;195(6):W447–W455.
78. Hastings MK, Mueller MJ, Woodburn J, et al. Acquired midfoot deformity and function in individuals with diabetes and peripheral neuropathy. Clin Biomech (Bristol, Avon) 2016;32(32):261–267.
79. Martín Noguerol T, Luna Alcalá A, Beltrán LS, Gómez Cabrera M, Broncano Cabrero J, Vilanova JC. Advanced MR Imaging Techniques for Differentiation of Neuropathic Arthropathy and Osteomyelitis in the Diabetic Foot. RadioGraphics 2017;37(4):1161–1180.
80. Johnson KA, Strom DE. Tibialis posterior tendon dysfunction. Clin Orthop Relat Res 1989 (239):196–206.
81. Haddad SL, Myerson MS, Younger A, Anderson RB, Davis WH, Manoli A 2nd. Symposium: Adult acquired flatfoot deformity. Foot Ankle Int 2011;32(1):95–111.
82. Nery C, Lemos AVKC, Raduan F, Mansur NSB, Baumfeld D. Combined Spring and Deltoid Ligament Repair in Adult-Acquired Flatfoot. Foot Ankle Int 2018;39(8):903–907.
83. Hill K, Saar WE, Lee TH, Berlet GC. Stage II flatfoot: what fails and why. Foot Ankle Clin 2003;8(1):91–104.
84. van Ooij B, Vos CJ, Saouti R. Arthroereisis of the subtalar joint: an uncommon complication and literature review. J Foot Ankle Surg 2012;51(1):114–117.
85. Matsumoto T, Chang SH, Takeda R, Tanaka S, Juji T. Bilateral Stress Fractures of the Talus Associated with Adult-Acquired Flatfoot Deformities. Case Rep Orthop 2018;2018:5376384.
86. Rozansky A, Varley E, Moor M, Wenger DR, Mubarak SJ. A radiologic classification of talocalcaneal coalitions based on 3D reconstruction. J Child Orthop 2010;4(2):129–135.
87. Mosca VS. Subtalar coalition in pediatrics. Foot Ankle Clin 2015;20(2):265–281.
88. Oburu E, Myerson MS. Deltoid Ligament Repair in Flatfoot Deformity. Foot Ankle Clin 2017;22(3):503–514.